nature methods

ARTICLES

https://doi.org/10.1038/s41592-020-0929-2

Live-cell super-resolved PAINT imaging of piconewton cellular traction forces

Joshua M. Brockman[1,7], Hanquan Su[2,7], Aaron T. Blanchard[1], Yuxin Duan[2], Travis Meyer[1], M. Edward Quach[3], Roxanne Glazier[1], Alisina Bazrafshan[2], Rachel L. Bender[2], Anna V. Kellner[1], Hiroaki Ogasawara[2], Rong Ma[2], Florian Schueder[4,5], Brian G. Petrich[3], Ralf Jungmann[4,5], Renhao Li[3], Alexa L. Mattheyses[6], Yonggang Ke[1,2] and Khalid Salaita[1,2] ✉

Despite the vital role of mechanical forces in biology, it still remains a challenge to image cellular force with sub-100-nm resolution. Here, we present tension points accumulation for imaging in nanoscale topography (tPAINT), integrating molecular tension probes with the DNA points accumulation for imaging in nanoscale topography (DNA-PAINT) technique to map piconewton mechanical events with ~25-nm resolution. To perform live-cell dynamic tension imaging, we engineered reversible probes with a cryptic docking site revealed only when the probe experiences forces exceeding a defined mechanical threshold (~7–21 pN). Additionally, we report a second type of irreversible tPAINT probe that exposes its cryptic docking site permanently and thus integrates force history over time, offering improved spatial resolution in exchange for temporal dynamics. We applied both types of tPAINT probes to map integrin receptor forces in live human platelets and mouse embryonic fibroblasts. Importantly, tPAINT revealed a link between platelet forces at the leading edge of cells and the dynamic actin-rich ring nucleated by the Arp2/3 complex.

Mechanical forces are vital to biology, regulating diverse processes including early development, platelet activation and immune function[1–3]. Force magnitude, orientation and dynamics influence cellular signaling outcomes[4]. Interestingly, force-transducing structures, such as filopodia, focal adhesions and the cellular cytoskeleton, are organized at the nanoscale and likely apply dynamic forces with nanoscale organization[5,6]. To better understand how mechanical forces are coupled to biochemical signaling pathways, methods are needed to map the nanoscale distribution of forces in living cells. However, to our knowledge, no technique is currently capable of dynamically mapping piconewton-scale forces with sub-100-nm resolution.

We and others have developed different types of molecular tension probes to map the piconewton forces applied by cells[7–10]. The most sensitive tension probes are composed of a DNA stem-loop hairpin flanked by a fluorophore-quencher pair[11–14]. Receptor forces unfold the stem-loop, separating the fluorophore from the quencher and producing a 20–100-fold increase in fluorescence[11]. In principle, one could directly image these probes using super-resolved imaging techniques such as stochastic optical reconstruction microscopy (STORM) or stimulated emission depletion (STED) microscopy, which routinely generate subdiffraction images of biological structures[15]; however, quenching processes and photobleaching make this technically challenging (Supplementary Note 1). Among the super-resolution techniques, DNA points accumulation for imaging in nanoscale topography (DNA-PAINT) has demonstrated the ability to resolve single molecular complexes at ~5-nm spatial resolution[16–19]. DNA-PAINT leverages transient binding of fluorophore-tagged 'imager' strands to complementary DNA 'docking' sequences to produce fluorescence blinking events amenable to single-molecule localization (Supplementary Fig. 1)[18]. Moreover, DNA-PAINT is robust to photobleaching and can be conducted in conditions that are favorable for live-cell imaging, making it suitable for capturing dynamic mechanical events. Theoretically, DNA-PAINT is also compatible with DNA tension probes because mechanical unfolding of the stem-loop reveals single-stranded DNA that could function as the docking sequence.

Results

To adapt our previously reported DNA-based molecular tension probes[11] for use with DNA-PAINT, we encoded a cryptic docking sequence within the stem region of the hairpin (Supplementary Table 1, Supplementary Fig. 2 and Supplementary Note 1) and performed DNA-PAINT measurements with this construct. The cryptic docking site is duplexed and hence concealed from binding to imager until cellular forces mechanically melt the duplex, thus exposing it and allowing for imager binding. To our surprise, DNA-PAINT performed poorly in imaging forces using the conventional stem-loop probe (Extended Data Fig. 1).

One potential reason for this poor performance is the mechanically strained nature of the docking sequence. Force spectroscopy studies show that mechanical strain creates a barrier for hybridization[20]. Accordingly, we developed a model[20,21] to explore the kinetics of imager hybridization to docking sites experiencing forces of 1–50 pN. Consistent with our observation, the model predicts that mechanical forces can impede imager binding (Extended Data Fig. 1 and Supplementary Note 2). Therefore, we designed and synthesized a strain-free tension-PAINT (sf-tPAINT) sensor to funnel

[1]Wallace H. Coulter Department of Biomedical Engineering, Georgia Institute of Technology and Emory University, Atlanta, GA, USA. [2]Department of Chemistry, Emory University, Atlanta, GA, USA. [3]Aflac Cancer and Blood Disorders Center, Children's Healthcare of Atlanta, Department of Pediatrics, Emory University, Atlanta, GA, USA. [4]Faculty of Physics and Center for Nanoscience, Ludwig Maximilian University, Munich, Germany. [5]Max Planck Institute of Biochemistry, Martinsried, Germany. [6]Department of Cell, Developmental, and Integrative Biology, University of Alabama at Birmingham, Birmingham, AL, USA. [7]These authors contributed equally: Joshua M. Brockman, Hanquan Su. ✉e-mail: k.salaita@emory.edu

mechanical force away from the docking site after probe opening (Fig. 1a,b, Supplementary Note 1, Supplementary Fig. 2 and Extended Data Fig. 1). In this design, the sf-tPAINT sensor functions as a force-triggered switch, exposing an unstrained cryptic docking sequence when receptor force, F, exceeds the probe $F_{1/2}$, which is defined as the equilibrium F that produces a 50% probability of unfolding. To test this design, we coated coverslips with cyclic-Arg-Gly-Asp (cRGD) sf-tPAINT probes labeled with Cy3B–BHQ2 and seeded human platelets onto these substrates. We used human platelets as a model because of their small size (2–5 µm), and the intimate link between mechanical forces and their clotting functions[22–24]. The Cy3B–BHQ2–sf-tPAINT probes reported platelet tension, and showed similar performance to conventional hairpin tension probes (Extended Data Fig. 1 and Supplementary Fig. 3).

Having validated that the sensor is functional in widefield microscopy, we next performed tPAINT on human platelet forces with sf-tPAINT probes lacking Cy3B–BHQ2 (Fig. 1c,d). Cells spread rapidly on the substrate, and, upon addition of 10 nM Cy3B imager in cell-imaging media, single-molecule fluorescence spots were observed under the cell-surface contact area (Supplementary Video 1). Platelets were imaged in total internal reflection fluorescence (TIRF) excitation mode at 5 Hz for 12 min. Localization of single Cy3B molecules using the Picasso software suite[17] revealed super-resolved maps of platelet 8.5-pN integrin forces (Fig. 1c,d and Extended Data Fig. 2). Additionally, the sf-tPAINT probe outperformed probes with strained docking sites, providing empirical support to our biophysical modeling (Supplementary Note 2 and Extended Data Fig. 1).

Integrin–ligand bond lifetimes are reported to be 0.1–20 s under force[25,26], which will lead to undersampling of mechanically strained probes in tPAINT (Supplementary Note 3). To reduce this effect, we employed the recently developed speed-optimized PAINT strategy[27] which maximizes the on-rate of imager sampling, thus better capturing short-lived mechanical events. Therefore, the data shown in Fig. 1c were collected with Tyrode's buffer supplemented with 37.5 mM Mg^{2+}, producing ~4-fold more localizations relative to experiments conducted in buffer without supplemental Mg^{2+}, and a signal-to-background ratio of 10 (Supplementary Fig. 4, Extended Data Fig. 3 and Fig. 1c,d). This allowed us to create a timelapse of platelet mechanics where each frame integrated 200 s of single-molecule localizations (Fig. 1c,d). Upon initial contact with the surface, cells spread (as observed by reflection interference contrast microscopy (RICM)) and then formed a 'ring' pattern of tension at the lamellipodial edge (Fig. 1c,d). The mechanical ring was highly dynamic, translocating 185 ± 75 nm over ~2–5 min (Supplementary Fig. 5). We quantified the ring width as 150 ± 80 nm (eight cells, $n = 3$ experiments; Supplementary Fig. 5). Two representative linescans are provided in Fig. 1e, demonstrating that the ring can be as thin as 90 nm. Additionally, we confirmed that the movement of the tPAINT signal coincides with the spread of the cell leading edge (Extended Data Fig. 4).

To demonstrate the generality of tPAINT, we imaged mouse embryonic fibroblasts (MEFs) stably expressing GFP-vinculin (MEF-GFP-vinculin) via tPAINT. Fibroblasts spread and formed focal adhesions (Fig. 1f). Following the addition of 10 nM Cy3B imager in media supplemented with 75 mM Mg^{2+}, we imaged the cell in TIRF excitation mode at 5 Hz to produce super-resolved maps of integrin tension (Fig. 1f and Extended Data Fig. 2). Tension was associated with focal adhesions and generally extended slightly beyond the distal tip of the focal adhesion footprint (Supplementary Fig. 3 and Extended Data Fig. 4), a finding consistent with previous diffraction-limited molecular tension measurements[28], and with traction force microscopy (TFM) measurements that found that the centroid of focal adhesion traction stresses was ~1 µm closer to the cell edge than the centroid of the focal adhesion itself[29]. Additionally, the number of tPAINT localizations was positively correlated with focal adhesion size and adhesion aspect ratio (Supplementary Fig. 6). We also confirmed that tPAINT is compatible with recent advances in computational super-resolution microscopy[30] by performing simultaneous tPAINT and super-resolution radial fluctuations (SRRF) (Supplementary Fig. 3), demonstrating a close connection between tPAINT localizations and GFP-vinculin.

To further accelerate the imager sampling rate of mechanically opened tPAINT probes, we screened different sf-tPAINT probe sequences based on speed-optimized[27] DNA-PAINT (Extended Data Fig. 5). Sequence-optimized probes enabled measurement of filopodial dynamics, revealed 100–200 nm of lateral movement of a fibroblast filopodium over 1–2 min and enabled measurement of the dynamics of filopodia retraction across a 180-s imaging window (Supplementary Fig. 7).

We found that the background signal was specific to the correct imager sequence, confirming that thermal breathing or probe impurities produce a small population of transiently open probes (Extended Data Fig. 6 and Supplementary Note 3). To address this issue, a kinetic filter and a Voronoi tessellation-based density filter[31] were used to suppress background (Extended Data Fig. 7). A detailed description of the filtering algorithm is provided in the Methods. An additional consideration in sf-tPAINT is tuning the image time window to maximize the number of localizations while also minimizing blurring of dynamic features such as the tension generated by filopodia or the leading edge of spreading cells (Supplementary Fig. 5 and Extended Data Fig. 8).

The 'ring'-like mechanical pattern of platelet integrin forces was consistent with the dimensions of high-density actin bundles that accumulate at the cell edge as observed by electron microscopy and fluorescence microscopy[32–34]. However, no technique is currently capable of sub-100-nm mapping of both traction forces and protein assemblies generating those forces. To address this need, we exploited multiplexed super-resolution imaging (Exchange-PAINT[18]), which switches out the imagers to super-resolve different targets. tPAINT was used to image 14-pN platelet integrin tension, then cells were fixed and stained with DNA-tagged phalloidin to allow Exchange-PAINT visualization of the actin cytoskeleton (Fig. 2a–d). The data showed a thin (330 ± 60 nm) ring of dense F-actin at the lamellipodial edge (Fig. 2c–f, seven platelets from two donors). Tension at the leading cell edge was highly coupled with this F-actin rim (Fig. 2e, white arrow); however, in some regions the tension lagged behind the F-actin edge (Fig. 2f, arrowhead). Since the cell

Fig. 1 | Super-resolved, live-cell imaging of integrin tension. a, Real-time sf-tPAINT probes composed of a ligand (blue) and an anchor (black) strand held together using a loop strand (green). When $F > F_{1/2}$, the stem opens, exposing a cryptic docking site for imager binding (orange). If $F < F_{1/2}$, then the probe refolds, and the docking site is concealed. **b**, Schematic and energy diagram comparing imager binding to conventional (strained) tension probes and sf-tPAINT probes. **c**, Timeseries showing sf-tPAINT of 8.5-pN integrin forces during the process of platelet activation. RICM is shown in the inset. The first frame shows a diffraction-limited reconstruction/tPAINT overlay of the 800–1,000 s time bin. **d**, Color-coded timeseries showing dynamics of lamellipodial tension during spreading (region of interest (ROI) 1 indicated by dotted box). **e**, Representative expansions of lamellipodial edge tension along with linescans reporting FWHM of a Gaussian fit (red line) to a greyscale rendering of sf-tPAINT (800–1,000 s time bin). **f**, sf-tPAINT image of 8.5-pN MEF integrin tension. Image time bins are color-coded. GFP-vinculin fluorescence colocalizes with sf-tPAINT single-molecule localizations. The data shown are representative of $n = 3$ independent platelet experiments from three different donors (eight images) and $n = 4$ fibroblast experiments (ten images). AU, arbitrary units; FWHM, full-width at half-maximum.

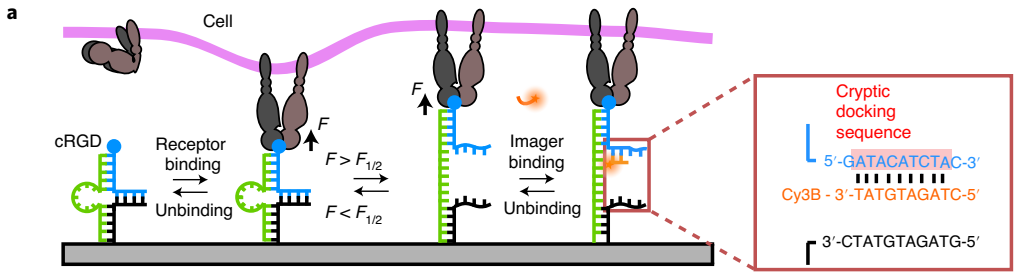
a
Cell
cRGD
Receptor binding
Unbinding
F
F > F1/2
F < F1/2
Imager binding
Unbinding
Cryptic docking sequence
5′-GATACATCTAC-3′
Cy3B - 3′-TATGTAGATC-5′
3′-CTATGTAGATG-5′

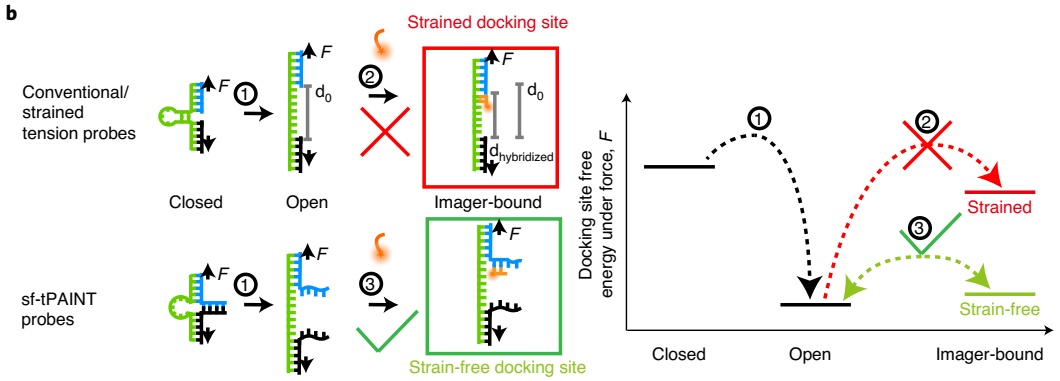
b
Strained docking site
Conventional/ strained tension probes
Closed
Open
Imager-bound
sf-tPAINT probes
Strain-free docking site
Docking site free energy under force, F
Strained
Strain-free
Closed
Open
Imager-bound

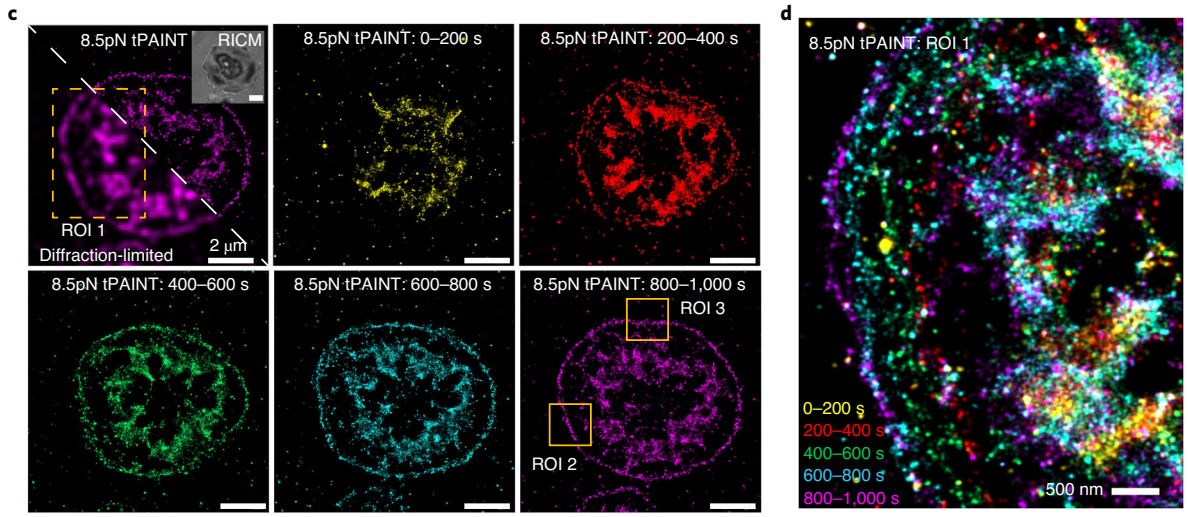
c
8.5pN tPAINT
RICM
ROI 1
Diffraction-limited
2 μm
8.5pN tPAINT: 0–200 s
8.5pN tPAINT: 200–400 s
8.5pN tPAINT: 400–600 s
8.5pN tPAINT: 600–800 s
8.5pN tPAINT: 800–1,000 s
ROI 3
ROI 2
d
8.5pN tPAINT: ROI 1
0–200 s
200–400 s
400–600 s
600–800 s
800–1,000 s
500 nm

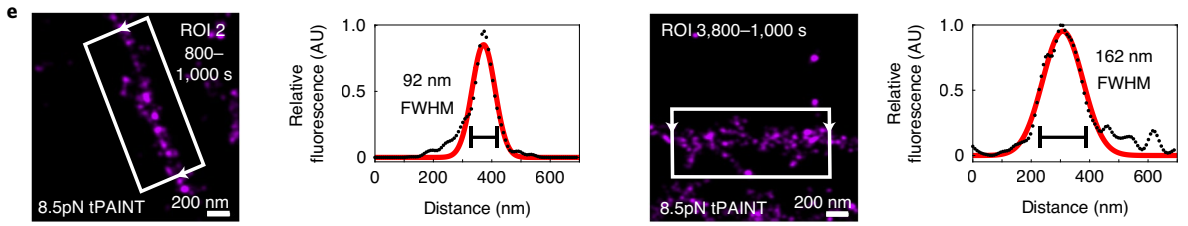
e
ROI 2
800–1,000 s
8.5pN tPAINT
200 nm
Relative fluorescence (AU)
92 nm FWHM
Distance (nm)
ROI 3,800–1,000 s
8.5pN tPAINT
200 nm
162 nm FWHM
Distance (nm)

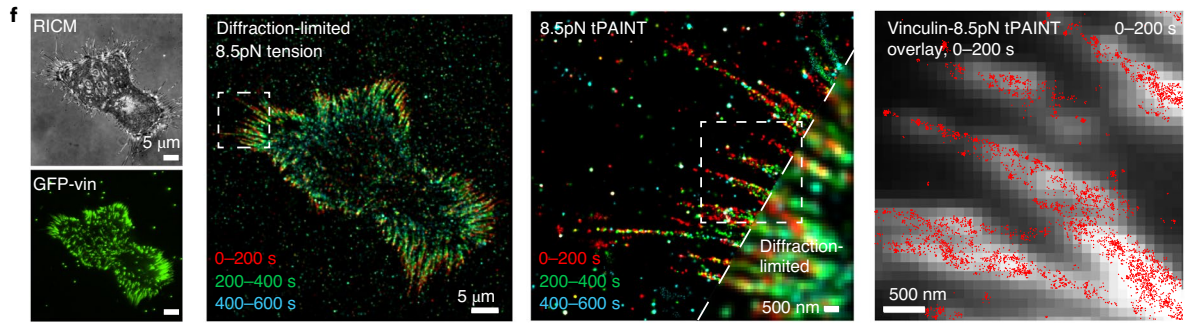
f
RICM
5 μm
GFP-vin
Diffraction-limited
8.5pN tension
0–200 s
200–400 s
400–600 s
5 μm
8.5pN tPAINT
0–200 s
200–400 s
400–600 s
Diffraction-limited
500 nm
Vinculin-8.5pN tPAINT overlay, 0–200 s
0–200 s
500 nm

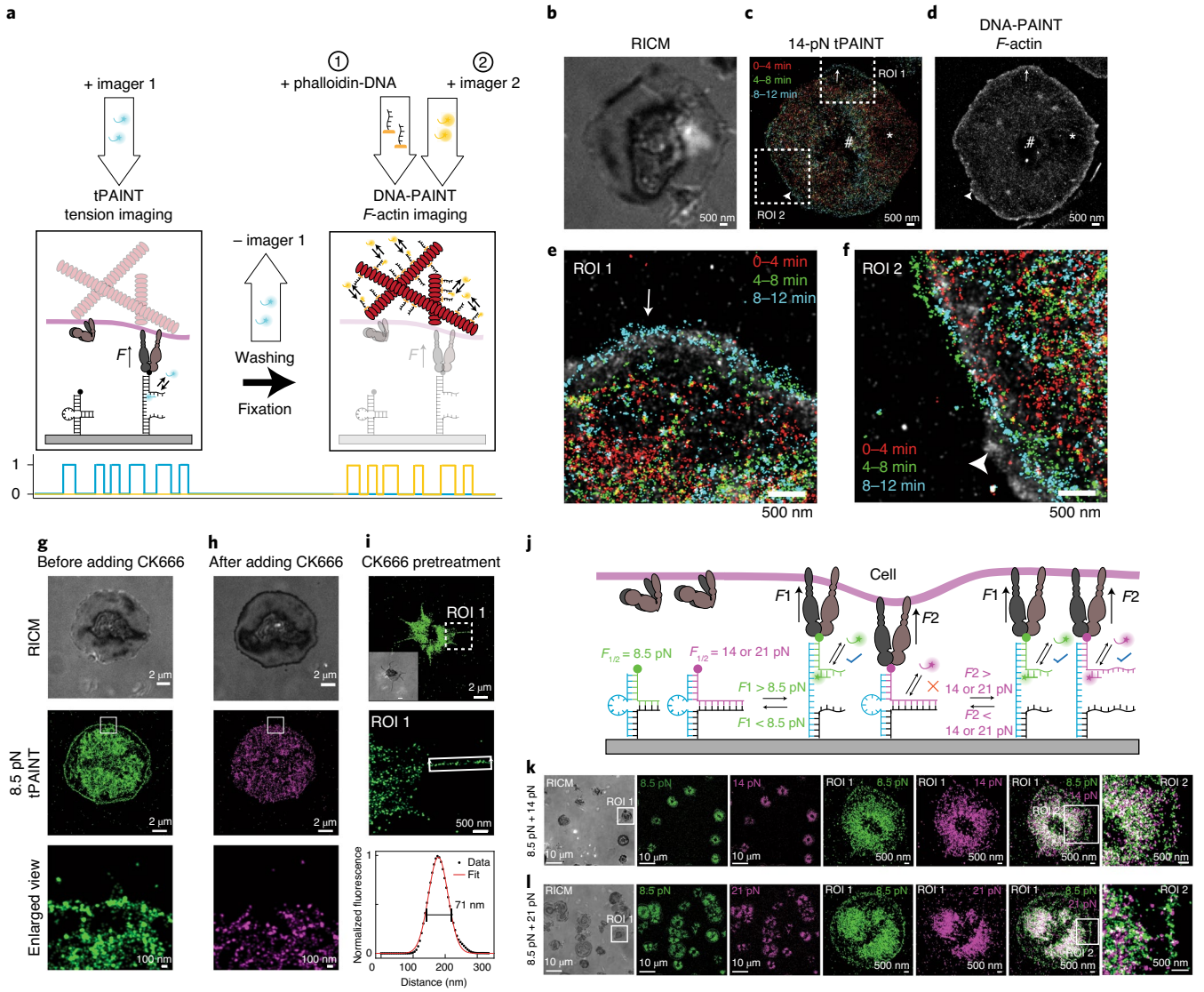

Fig. 2 | Platelet lamellipodial ring tension is driven by a thin ring of polymerizing actin. a, Platelet 14-pN integrin tension was imaged before fixation, staining and Exchange-PAINT was implemented to super-resolve the platelet actin cytoskeleton. **b**–**d**, RICM (**b**), time-resolved 14-pN tPAINT (**c**) and F-actin stained with DNA-tagged phalloidin (**d**). **e**,**f**, Enlarged view of tension at the lamellipodial edge for ROI 1 (**e**) and ROI 2 (**f**) reveals close association between tension and actin (white arrow). In some regions (**f**), actin polymerization extends beyond tension (arrowhead). Note that an area of depleted actin (denoted with an asterisk) corresponds to an area where tension receded after 4 min. The hash indicates a fiducial marker. Actin-tension data are representative of seven platelets from $n = 2$ independent experiments. Note that tension-actin overlay images use higher contrast for tension than F-actin because F-actin localization density is higher than tension localization density. **g**,**h**, Platelet tension before (**g**) and after (**h**) treatment with the Arp2/3 inhibitor CK666. CK666 treatment (50 μM) removes platelet lamellipodial edge tension (two platelets) or prevents lamellipodial edge tension formation (seven platelets) (nine platelets total from $n = 2$ independent experiments). **i**, Platelets pretreated with 50 μM CK666 spread slowly, utilize filopodia to engage with the cRGD substrate and do not exhibit lamellipodial edge tension (18 platelets from $n = 3$ independent experiments). **j**, Force-multiplexed tPAINT is possible by coating surfaces with two probes with distinct $F_{1/2}$ values. **k**,**l**, Force-multiplexed tPAINT images of 8.5 and 14 pN (**k**) and 8.5 and 21 pN (**l**) forces reveal that lamellipodial edge tension exceeds 14 pN, but does not frequently exceed 21 pN. Integrin tension in the center of platelets exceeds 21 pN. The data shown for force-multiplexed tPAINT are representative of $n = 3$ independent experiments.

edge protruded rapidly in some cases (white arrow, Fig. 2d,e), it is possible that regions where the tension lagged behind the actin rim are areas of rapid actin polymerization in which the tension has not yet advanced to the ring edge.

We posited that the cell edge tension is driven by Arp2/3-mediated branching actin polymerization, as loss of branching polymerization causes platelets to lose lamellipodia[35], and Arp2/3 localizes to the lamellipodial edge of spreading platelets[36]. Treating platelets with 50 μM CK666 (an Arp2/3 inhibitor) abolished platelet lamellipodial rim tension in two platelets, while seven other platelets failed to develop lamellipodial ring tension (nine platelets from $n = 2$ experiments, Fig. 2g,h and Extended Data Fig. 9). The spatially selective action of Arp2/3 inhibition can only be resolved using tPAINT as the tension-ring structure is ~150-nm wide, not detectable using state-of-art TFM (Supplementary Table 4 and Supplementary Fig. 8). Pretreating platelets with 50 μM CK666 for 30 min before seeding slowed platelet spreading, abolished the formation of the rim tension and often produced platelets with prominent filopodia (Fig. 2i and Extended Data Fig. 9). Treating platelets with the myosin light chain kinase inhibitor ML-7 led to a decrease in 8.5-pN

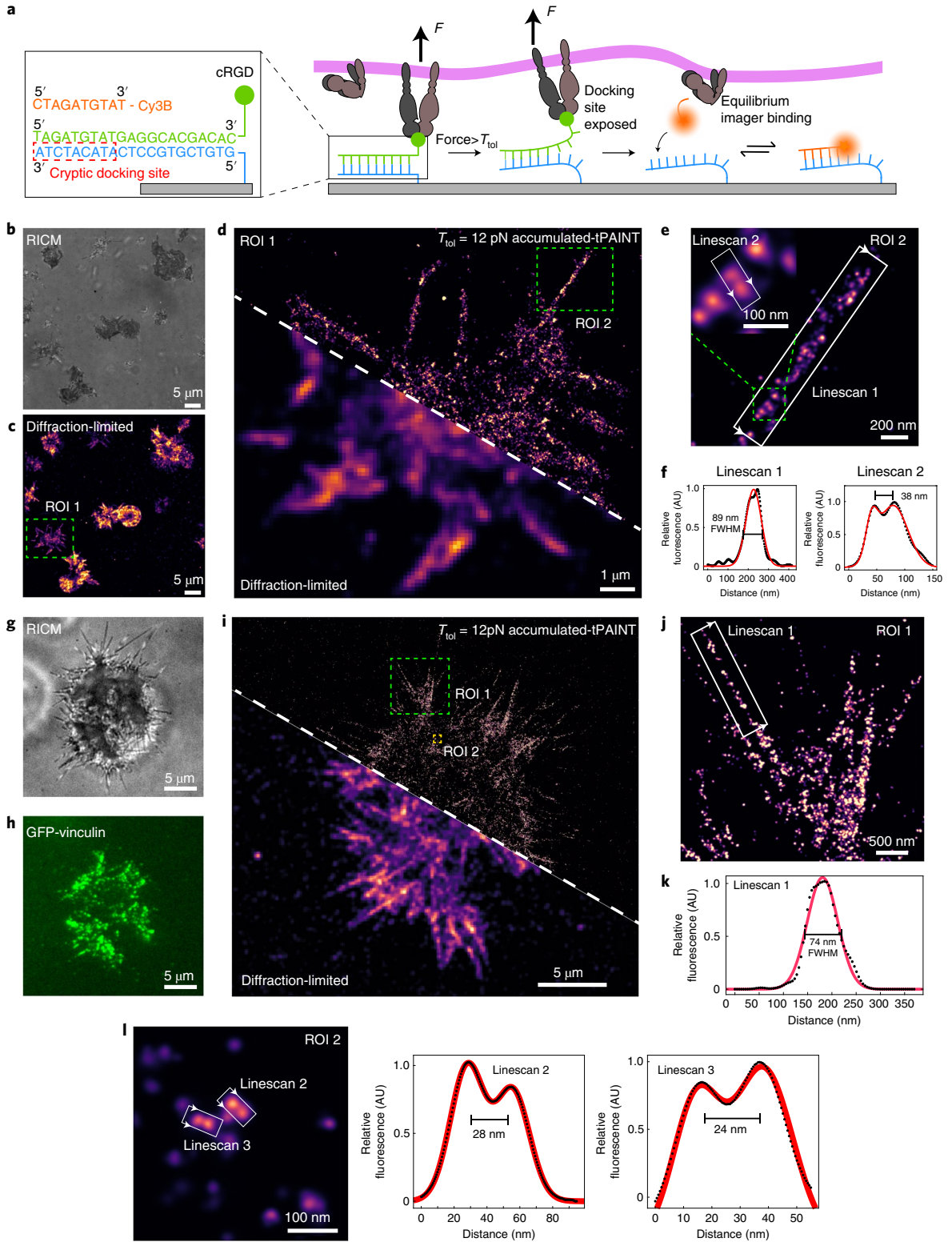

Fig. 3 | Accumulated-tPAINT enables high-resolution tension imaging. a, Schematic showing mechanism of accumulated-tPAINT. When integrin $F > T_{tol}$, the probe ruptures, exposing a cryptic docking site. Cy3B imager strands transiently bind to this exposed site to report the cellular traction force footprint. **b**,**c**, RICM (**b**) and diffraction-limited reconstruction (**c**) 12-pN tension map of platelets seeded on the surface for 25 min. Color indicates the localization density. **d**, Overlay of accumulated-tPAINT image with the diffraction-limited reconstruction. **e**, Enlarged view of the green ROI noted in **d**. **f**, Linescans of structures indicated in (**e**). The direction of the linescan is depicted using white arrows. Red fit is based on a Gaussian with FWHM shown on plots. **g**,**h**, RICM (**g**) and GFP-vinculin (**h**) images of MEF cells on an accumulated-tPAINT surface for ~25 min. **i**, 12-pN accumulated-tPAINT and diffraction-limited overlay. **j**, Enlarged view of ROI indicated by the green rectangle in **i**. **k**, Linescan across the filopodial tension indicated by ROI in **j**. **l**, 12-pN tension hot spots that are separated by 24 and 28 nm. The platelet data shown are representative of $n = 8$ replicates (22 images) while the fibroblast data are representative of $n = 9$ replicates (24 images).

mechanical events across the entire cell footprint, including in the cell center (Extended Data Fig. 9). Finally, we performed two-color force-multiplexed tPAINT (Fig. 2j) to characterize spatial variations in platelet forces and found that the lamellipodial edge tension is generally less than 21 pN (Fig. 2k,l), further distinguishing force generation at the edge from the platelet body.

Due to the short integrin–ligand bond lifetimes (~0.1–20 s), tPAINT will not fully record all receptor-mediated mechanical events even when utilizing speed-optimized PAINT (elevated Mg^{2+} and sequence-optimized probes). To eliminate this potential issue of undersampling mechanically opened probes, we employed DNA tension probes that rupture irreversibly under force. These probes, inspired by the tension gauge tether originally developed by Wang and Ha[37], enable accumulated-tPAINT imaging (Fig. 3a). Accumulated-tPAINT probes are composed of a DNA duplex, with one oligonucleotide anchored to the substrate while the other was modified with cRGD. The anchored strand also contained a cryptic 9-base pair docking sequence. The probe ruptures irreversibly when F exceeds the mechanical stability of the duplex (T_{tol}), exposing a cryptic docking sequence and allowing imager binding (Fig. 3a). Because these duplexes rupture irreversibly, imagers repeatedly sample the exposed cryptic binding sites, generating accumulated-tPAINT images of the force 'history' of mechanical events where $F > T_{tol}$.

We seeded human platelets on the $T_{tol} = 12$-pN accumulated-tPAINT surface (Fig. 3b) and, after ~10 min, performed accumulated-tPAINT. Platelets were imaged in TIRF excitation mode at 5 Hz over a duration of 25 min with 2.5 nM Cy3B imager. As expected, single-molecule Cy3B imager localizations were enhanced at the platelet-surface contact area (Supplementary Video 2 and Extended Data Figs. 2 and 3), with an average signal-to-background enhancement ratio of ~17. Overlaying the diffraction-limited reconstruction (Fig. 3c) with the accumulated-tPAINT image validated the improved resolution (Fig. 3d). Specifically, we identified the tension footprint of a platelet filopodium measuring 89 nm in width (Fig. 3e,f). The platelet data shown in Fig. 3 were collected with ~10-nm (0.09 pixel) precision (determined by nearest-neighbor analysis[38], Supplementary Fig. 9), matching the typical precision metrics for DNA-PAINT[39].

We also produced accumulated-tPAINT maps of MEF traction forces (Fig. 3g–l), showing filopodial-generated tension ~74 nm in width (Fig. 3j,k). Because accumulated-tPAINT maps static features, its resolution is likely akin to the resolution of conventional DNA-PAINT. We were able to resolve ruptured probes separated by ~25 nm within the MEF tension footprint (Fig. 3i). To determine the potential spatial resolution of tPAINT, we characterized the distribution of tension probes on the surface (Extended Data Fig. 10). The density of probes on the surface was $2{,}364 \pm 255$ probes per μm^2, suggesting that probes may be spaced as closely as 20 nm apart on the surface. DNA-PAINT imaging of a surface coated with open docking sites showed that probes are not evenly distributed; thus probe distribution likely sets the spatial resolution of tPAINT (Extended Data Fig. 10). Using other types of chemistry to immobilize probes more uniformly and densely on the coverslip may further improve the spatial resolution of tPAINT[40].

Discussion

The current standard technique for measuring cellular forces is TFM, which calculates traction stresses in deformable polymer films with ~700-nm spatial resolution[29,41,42] (Supplementary Table 4). tPAINT offers a complementary approach, mapping molecular (piconewton) mechanical events with up to 25-nm resolution. In the context of molecular tension probes, a single report used Bayesian analysis of blinking and bleaching (3B) imaging for super-resolved mechanical measurements, but 3B is computationally intensive, susceptible to photobleaching, not suitable for long-term cellular imaging and offers lower spatial resolution[43,44].

A key concept in tPAINT is mechano-selection[22] which is the substantially enhanced (over an order of magnitude) binding of imager to mechanically triggered probes over background. Therefore, it is important that tPAINT probes are thermally stable enough to avoid excessive background signal due to (nonmechanical) probe breathing. Extended Data Fig. 3 and Extended Data Fig. 6 quantify background localizations in tPAINT and underscore this point. The sf-tPAINT probes provide a means of super-resolved dynamic measurements of cellular forces. This is a key feature, because the magnitude, spatial organization, timing, frequency and history of forces influence signaling outcomes, as was recently shown in T cells[45] and in fibroblast adhesions[46]. The likelihood of capturing mechanical events in sf-tPAINT depends on bond lifetime and force lifetime in relation to the imager sampling rate, which may be up to ~0.3 s^{-1} in speed-optimized PAINT[27].

Given that accumulated-tPAINT probes rupture irreversibly, this probe offers high spatial resolution with potentially unlimited sampling of force-exposed docking sites. This improved resolution will be important in imaging fixed samples, where temporal information is not needed and where Exchange-tPAINT is integrated in the workflow.

To demonstrate the capabilities of tPAINT we have mapped platelet and fibroblast integrin tension, revealing dynamic nanoscale features, such as a rim of tension at the spreading edge of platelets and scanning filopodial tension. We also demonstrate two types of multiplexed tPAINT: mapping two thresholds of tension simultaneously or alternatively by performing Exchange-tPAINT to correlate integrin tension with the F-actin architecture driving it. Pharmacological studies confirm that platelet lamellipodial tension is driven by the Arp2/3 complex mediating actin branching. This ability to simultaneously super-resolve mechanical events and cytoskeletal structure is powerful; thus, we anticipate that tPAINT will become a workhorse tool linking structural biology to mechanobiology. One limitation in tPAINT is the lack of orientation information, but this limitation will likely be resolved upon integration of recently developed cellular force polarization imaging techniques to reveal three-dimensional force vectors of DNA probes[22,47]. Another limitation can be summarized as a trade-off between time and resolution. Real-time imaging undersamples mechanical events but offers dynamical information in live cells; conversely, accumulated-tPAINT will sample all mechanical events at the cost of temporal resolution. Future speed optimizations in PAINT will alleviate this trade-off, enabling molecular force imaging combined with spatial mapping of the cell's machinery in real-time.

Online content

Any methods, additional references, Nature Research reporting summaries, source data, extended data, supplementary information, acknowledgements, peer review information; details of author contributions and competing interests; and statements of data and code availability are available at https://doi.org/10.1038/s41592-020-0929-2.

Received: 18 December 2019; Accepted: 20 July 2020;
Published online: 14 September 2020

References

1. Discher, D. E., Janmey, P. & Wang, Y. L. Tissue cells feel and respond to the stiffness of their substrate. *Science* **310**, 1139–1143 (2005).
2. Qiu, Y. et al. Platelet mechanosensing of substrate stiffness during clot formation mediates adhesion, spreading, and activation. *Proc. Natl Acad. Sci. USA* **111**, 14430–14435 (2014).
3. Liu, Y. et al. DNA-based nanoparticle tension sensors reveal that T-cell receptors transmit defined pN forces to their antigens for enhanced fidelity. *Proc. Natl Acad. Sci. USA* **113**, 5610–5615 (2016).

4. Brockman, J. M. & Salaita, K. Mechanical proofreading: a general mechanism to enhance the fidelity of information transfer between cells. *Front. Phys.* **7**, 14 (2019).
5. Kanchanawong, P. et al. Nanoscale architecture of integrin-based cell adhesions. *Nature* **468**, 580–584 (2010).
6. Spiess, M. et al. Active and inactive β1 integrins segregate into distinct nanoclusters in focal adhesions. *J. Cell Biol.* **217**, 1929–1940 (2018).
7. Stabley, D. R., Jurchenko, C., Marshall, S. S. & Salaita, K. S. Visualizing mechanical tension across membrane receptors with a fluorescent sensor. *Nat. Methods* **9**, 64–67 (2012).
8. Liu, Y., Yehl, K., Narui, Y. & Salaita, K. Tension sensing nanoparticles for mechano-imaging at the living/nonliving interface. *J. Am. Chem. Soc.* **135**, 5320–5323 (2013).
9. Galior, K., Liu, Y., Yehl, K., Vivek, S. & Salaita, K. Titin-based nanoparticle tension sensors map high-magnitude integrin forces within focal adhesions. *Nano Lett.* **16**, 341–348 (2016).
10. Grashoff, C. et al. Measuring mechanical tension across vinculin reveals regulation of focal adhesion dynamics. *Nature* **466**, 263–266 (2010).
11. Zhang, Y., Ge, C., Zhu, C. & Salaita, K. DNA-based digital tension probes reveal integrin forces during early cell adhesion. *Nat. Commun.* **5**, 5167 (2014).
12. Blakely, B. L. et al. A DNA-based molecular probe for optically reporting cellular traction forces. *Nat. Methods* **11**, 1229 (2014).
13. Blanchard, A. T. & Salaita, K. Emerging uses of DNA mechanical devices. *Science* **365**, 1080–1081 (2019).
14. Ma, V. P.-Y. & Salaita, K. DNA nanotechnology as an emerging tool to study mechanotransduction in living systems. *Small* **15**, 1900961 (2019).
15. Sahl, S. J., Hell, S. W. & Jakobs, S. Fluorescence nanoscopy in cell biology. *Nat. Rev. Mol. Cell Biol.* **18**, 685–701 (2017).
16. Dai, M., Jungmann, R. & Yin, P. Optical imaging of individual biomolecules in densely packed clusters. *Nat. Nanotechnol.* **11**, 798–807 (2016).
17. Schnitzbauer, J., Strauss, M. T., Schlichthaerle, T., Schueder, F. & Jungmann, R. Super-resolution microscopy with DNA-PAINT. *Nat. Protoc.* **12**, 1198–1228 (2017).
18. Jungmann, R. et al. Multiplexed 3D cellular super-resolution imaging with DNA-PAINT and Exchange-PAINT. *Nat. Methods* **11**, 313–318 (2014).
19. Jayasinghe, I. et al. True molecular scale visualization of variable clustering properties of ryanodine receptors. *Cell Rep.* **22**, 557–567 (2018).
20. Whitley, K. D., Comstock, M. J. & Chemla, Y. R. Elasticity of the transition state for oligonucleotide hybridization. *Nucleic Acids Res.* **45**, 547–555 (2017).
21. Woodside, M. T. et al. Nanomechanical measurements of the sequence-dependent folding landscapes of single nucleic acid hairpins. *Proc. Natl Acad. Sci. USA* **103**, 6190–6195 (2006).
22. Brockman, J. M. et al. Mapping the 3D orientation of piconewton integrin traction forces. *Nat. Methods* **15**, 115–118 (2018).
23. Zhang, Y. et al. Platelet integrins exhibit anisotropic mechanosensing and harness piconewton forces to mediate platelet aggregation. *Proc. Natl Acad. Sci. USA* **115**, 325–330 (2018).
24. Ting, L. H. et al. Contractile forces in platelet aggregates under microfluidic shear gradients reflect platelet inhibition and bleeding risk. *Nat. Commun.* **10**, 1204 (2019).
25. Chen, Y. et al. An integrin $\alpha_{IIb}\beta_3$ intermediate affinity state mediates biomechanical platelet aggregation. *Nat. Mater.* **18**, 760–769 (2019).
26. Kong, F., Garcia, A. J., Mould, A. P., Humphries, M. J. & Zhu, C. Demonstration of catch bonds between an integrin and its ligand. *J. Cell Biol.* **185**, 1275–1284 (2009).
27. Schueder, F. et al. An order of magnitude faster DNA-PAINT imaging by optimized sequence design and buffer conditions. *Nat. Methods* **16**, 1101–1104 (2019).
28. Liu, Y. et al. Nanoparticle tension probes patterned at the nanoscale: impact of integrin clustering on force transmission. *Nano Lett.* **14**, 5539–5546 (2014).
29. Plotnikov, S. V., Pasapera, A. M., Sabass, B. & Waterman, C. M. Force fluctuations within focal adhesions mediate ECM-rigidity sensing to guide directed cell migration. *Cell* **151**, 1513–1527 (2012).
30. Gustafsson, N. et al. Fast live-cell conventional fluorophore nanoscopy with ImageJ through super-resolution radial fluctuations. *Nat. Commun.* **7**, 12471 (2016).
31. Levet, F. et al. SR-Tesseler: a method to segment and quantify localization-based super-resolution microscopy data. *Nat. Methods* **12**, 1065–1071 (2015).
32. Mayr, S. et al. Localization microscopy of actin cytoskeleton in human platelets. *Int. J. Mol. Sci.* **19**, 1150 (2018).
33. Bearer, E. L., Prakash, J. M. & Li, Z. Actin dynamics in platelets. *Int. Rev. Cytol.* **217**, 137–182 (2002).
34. Hartwig, J. H. Mechanisms of actin rearrangements mediating platelet activation. *J. Cell Biol.* **118**, 1421–1442 (1992).
35. Gaertner, F. et al. Migrating platelets are mechano-scavengers that collect and bundle bacteria. *Cell* **171**, e1323 (2017).
36. Li, Z., Kim, E. S. & Bearer, E. L. Arp2/3 complex is required for actin polymerization during platelet shape change. *Blood* **99**, 4466–4474 (2002).
37. Wang, X. & Ha, T. Defining single molecular forces required to activate integrin and notch signaling. *Science* **340**, 991–994 (2013).
38. Endesfelder, U., Malkusch, S., Fricke, F. & Heilemann, M. A simple method to estimate the average localization precision of a single-molecule localization microscopy experiment. *Histochem. Cell Biol.* **141**, 629–638 (2014).
39. Strauss, S. et al. Modified aptamers enable quantitative sub-10-nm cellular DNA-PAINT imaging. *Nat. Methods* **15**, 685–688 (2018).
40. Li, J. et al. Exploring the speed limit of toehold exchange with a cartwheeling DNA acrobat. *Nat. Nanotechnol.* **13**, 723–729 (2018).
41. Polacheck, W. J. & Chen, C. S. Measuring cell-generated forces: a guide to the available tools. *Nat. Methods* **13**, 415–423 (2016).
42. Colin-York, H. et al. Super-resolved traction force microscopy (STFM). *Nano Lett.* **16**, 2633–2638 (2016).
43. Cox, S. et al. Bayesian localization microscopy reveals nanoscale podosome dynamics. *Nat. Methods* **9**, 195–200 (2011).
44. Morimatsu, M., Mekhdjian, A. H., Chang, A. C., Tan, S. J. & Dunn, A. R. Visualizing the interior architecture of focal adhesions with high-resolution traction maps. *Nano Lett.* **15**, 2220–2228 (2015).
45. Pryshchep, S., Zarnitsyna, V. I., Hong, J., Evavold, B. D. & Zhu, C. Accumulation of serial forces on TCR and CD8 frequently applied by agonist antigenic peptides embedded in MHC molecules triggers calcium in T cells. *J. Immunol.* **193**, 68–76 (2014).
46. Elosegui-Artola, A. et al. Mechanical regulation of a molecular clutch defines force transmission and transduction in response to matrix rigidity. *Nat. Cell Biol.* **18**, 540–548 (2016).
47. Blanchard, A. T., Brockman, J. M., Salaita, K. & Mattheyses, A. L. Variable incidence angle linear dichroism (VALiD): a technique for unique 3D orientation measurement of fluorescent ensembles. *Opt. Express* **28**, 10039–10061 (2020).

Methods

Materials. Cy3B-NHS ester (PA63101) was acquired from GE Healthcare Life Sciences. DNA was custom synthesized by Integrated DNA Technologies. Cyclo[Arg-Gly-Asp-d-Phe-Lys(PEG-PEG)] (PCI-3696-PI), elsewhere abbreviated as cRGD, was acquired from Peptides International. Streptavidin (S000–01) was obtained from Rockland-Inc. µ-Slide VI$^{0.4}$ six-channel slides (80606) and 25 × 75 mm^2 glass coverslips (10812) were purchased from Ibidi. N-hydroxyl succinimide-5 kDa PEG-biotin (NHS-PEG-biotin, HE041024–5K) was purchased from Biochempeg. N-hydroxyl succinimide-5kDa mPEG (NHS-mPEG, PG1-SC-5k-1) was purchased from Nanocs. Sulfo-N-hydroxyl succinimide-acetate (sulfo-NHS-acetate, 26777) was purchased from Thermo-Fisher. (3-Aminopropyl)triethoxysilane (APTES, 440140, 99% purity) was purchased from Sigma-Aldrich. TetraSpeck beads were purchased from Thermo-Fisher (T7279). Phalloidin-amine was purchased from Santa-Cruz Biotechnology (sc-397330). All other reagents and materials (unless otherwise stated) were purchased from Sigma-Aldrich and used without purification. All buffers were prepared with 18.2-MΩ nanopure water.

Surface preparation. tPAINT surface preparation was modified from previously published protocols[3]. Briefly, rectangular glass coverslips (25 × 75 mm^2) were cleaned using piranha solution. Caution: piranha can be explosive when mixed with organics. The piranha solution was prepared using a 1:3 mixture of H_2O_2 and H_2SO_4. Slides were then washed in six successive beakers of nanopure water and then etched in a beaker of KOH (0.5 M) for 1 h in an ice-filled sonicator. The coverslips were washed six times using nanopure water, followed by three successive washes using ethanol. In a separate beaker of ethanol, slides were reacted with 3% v/v APTES for 1 h. Coverslips were then washed three times with ethanol and dried under a stream of N_2 gas. Slides were then reacted with cloud-point NHS-PEG-biotin (10% w/v) for 1 h in 0.5 M K_2SO_4 and 0.1 M $NaHCO_3$ (pH 9). Next, slides were washed three times with nanopure water and reacted for 30 min with NHS-mPEG (5% w/v) and sulfo-NHS-acetate (1% w/v) in 0.5 M K_2SO_4 and 0.1 M $NaHCO_3$ (pH 9) to consume any unreacted amines on the surface. Slides were dried under N_2 gas, and then stored at −80 °C for up to 2 weeks before use.

Imaging chamber assembly. Before imaging, the µ-Slide VI$^{0.4}$ six-channel slide was adhered on the 5 kDa PEG-biotin surface. To further reduce nonspecific DNA binding during the imaging, the micro-channels were passivated with 5% v/v Tween 20 in 10 mM Tris buffer, pH 8, with 50 mM NaCl for 15–30 min (refs. [48,49]). The channels were washed with 1× PBS and filled with 50 µg ml^{-1} streptavidin for a 1-h incubation. The channels were then washed with 1× PBS and incubated with 1 µM DNA probe solutions for 1 h. For force-multiplexing experiments, the surfaces were incubated with two tension probes, each at 1 µM concentration. Finally, the channels were washed with cell-imaging buffer before imaging (Tyrode's buffer for platelets, FluoroBrite DMEM Media, A1896701, Thermo-Fisher for fibroblast experiments).

DNA hybridization. DNA oligonucleotides were hybridized at 200 nM or 2 µM in a 0.2-ml Thermowell tube. DNA was heated to 90 °C and then cooled at a rate of 1.3 °C min^{-1} to 35 °C.

Platelet handling. Venous blood was obtained from healthy adult human volunteers by venipuncture into 3.8% trisodium citrate. Human platelet-rich plasma was prepared via centrifugation (12 min, 140*g*) of whole blood. Platelet-rich plasma was collected following the spin, diluted to 10 ml in PIPES saline and treated with 12 µl of PGE1 (500 µM) to prevent platelet activation. The solution was inverted gently several times to mix the PGE1 into solution and then centrifuged at 1,900*g* for 8 min. The supernatant was discarded, and the platelets were resuspended in 400 µl of Tyrode's buffer for 5 min before an additional 600 µl of Tyrode's buffer was added and mixed gently to resuspend the platelet pellet. Platelets were incubated at room temperature for at least 30 min before beginning experiments.

Cell culture. MEFs were cultured according to American Type Culture Collection guidelines. Briefly, cells were cultured in DMEM supplemented with penicillin/streptomycin and 15% fetal bovine serum (v/v). Cells were passaged every 2–3 d as required.

Single-molecule localization imaging for tPAINT. Imaging was accomplished on a Nikon Eclipse Ti microscope, operated by Nikon Elements software, using a 1.49 numerical aperture (NA) CFI Apo ×100 objective, perfect focus system and a TIRF laser launch with 75 mW and 561 nm. A Chroma quad cube (ET-405/488/561/640 nm Laser Quad Band) and an RICM (Nikon: 97270) cube were used for imaging. Widefield epifluorescence illumination was provided by an X-Cite 120 lamp (Excelitas). An Andor iXon Ultra 897 electron-multiplying charge-coupled device was used for image acquisition. Lasers were operated in TIRF mode for all acquisitions.

Images were acquired using RAM capture via a Nikon Fast Timelapse acquisition. Cameras were operated at 17-MHz refresh rate with an electron-multiplying gain of 300 and a 200-ms exposure time. A ×1.5 lens introduced into the optical path allowed imaging with a pixel size of 110 nm. For time-resolved measurements, Nikon JOBS was used to alternate between capturing 300 frames of single-molecule fluorescence signal and then one RICM image and one epifluorescence GFP image, enabling tracking of the cell position via widefield microscopy throughout the acquisition. The individual 300-frame single-molecule image stacks were then stitched back together and analyzed in Picasso. Four-color TetraSpeck beads were used as fiducial markers.

For force-multiplexing experiments data were acquired using the same microscope described in this section with the following modifications: orthogonal DNA imagers labeled with Atto 488 and Cy3B were employed, single-molecule localizations were collected simultaneously utilizing an Andor Tucam system with dual iXon Ultra 897 electron-multiplying charge-coupled devices, and fluorophores were excited simultaneously with 488-nm and 561-nm TIRF illumination.

The exact imaging conditions used for all images in the main text are provided in Supplementary Table 3.

Exchange-tPAINT. tPAINT imaging of the platelet integrin tension was acquired before fixation with 37.5 mM Mg^{2+} and 7.5 nM Cy3B imager. The cells were then fixed with 4% formaldehyde solution on the microscope for 10 min without disturbing the sample. The channel was washed three times with 1× PBS, and cells were permeabilized with 0.1% Triton X-100 in 1× PBS for 5 min at room temperature. After permeabilization, the cells were stained with 1 µM phalloidin tagged with a DNA dock for 15 min and the channel was gently washed with imaging buffer three times. Lastly, Cy3B imager strand complementary to the phalloidin-DNA dock was added at 1 nM for F-actin imaging. F-actin DNA-PAINT images were acquired at 5 Hz for 60 min. Actin and tPAINT images were registered using tetraspeck beads as fiducial markers in Picasso.

Image processing. Image processing was performed in MATLAB 2019a (MathWorks) and in Picasso[17], a software that is freely available via the Jungmann laboratory website. The bioformats toolbox enabled direct transfer of Nikon Elements image files (.nd2) into the MATLAB environment. Drift correction was performed in Picasso by several consecutive rounds of redundant cross correlation. All 'diffraction-limited' reconstructions displayed in this paper were created in Picasso by convolving the single-molecule localizations with a 1-pixel Gaussian blur to mimic the point spread function of the microscope.

Due to the presence of background, nonmechanical signal from sf-tPAINT probe 'breathing' during experiments, it is necessary to filter the tPAINT single-molecule localization data. Accordingly, we employed filtering algorithms to distinguish between force-mediated signal and background signal (Extended Data Fig. 7). Briefly, we applied a kinetic filter to eliminate localizations associated with surface defects, dust or other contaminants on the surface. These localizations possess brief dark times (very high apparent imager on rate, k_{on}) or prolonged bright times (very low imager off rate, k_{off}). To remove these localizations, the single-molecule localizations were binned into 3× oversampled pixels (3 oversampled pixels per 1 physical pixel on detector). Single localization events were identified as consecutive frames in which single-molecule localizations occurred within each oversampled pixel, or within its eight immediate neighbors. If more than 14 events occurred within 25 frames, all of the component events were removed from the dataset. This treatment does not alter the single-molecule events that originate from DNA–DNA binding because the expected dark time between single-molecule events is 10–100 s for 10 nM imager concentration; thus, multiple binding events within 5 s are unlikely. Additionally, the bond lifetime of the imager and the docking sites is too short to produce 14 consecutive bright frames. After the kinetic filter, we employed a Voronoi tessellation density filter to remove sparse localizations[31], reasoning that cell tension will produce denser localizations than the cell-free background (Extended Data Fig. 7). We computed the Voronoi tessellation of the single-molecule localization dataset and then assigned a first rank density to each point. A background density was calculated as the average localization density within a user-defined cell-free region of the substrate. We then removed all single-molecule localizations with a first rank density of less than 1–15× the background localization first rank density. This procedure may 'erode' edge localizations, sharpening spatial features; thus, it is important to use the lowest possible Voronoi density filter that produces high-quality images. The effects of different density filters are displayed in detail in Extended Data Fig. 7. A spatial density filter of 3× the background was employed for the data displayed in Fig. 1, a 2× filter for the data in Fig. 2 and a 5× density filter was employed for the data displayed in Fig. 3.

For Tucam experiments, including simultaneous tPAINT-SRRF and force multiplexing, the single-molecule localization lists were registered after single-molecule localization in MATLAB. Localizations corresponding to TetraSpeck beads were manually identified and used as fiducial markers to apply a projective registration to the single-molecule dataset.

Synthesis. The sequences of all strands are provided in Supplementary Table 1. Briefly, 100 nmol of c(RGDfK(PEG-PEG)) was reacted with approximately 150 nmol of NHS-azide in dimethylsulfoxide overnight. cRGD-N_3 was purified via reverse-phase HPLC with a Grace Alltech C18 column (1 ml min^{-1} flow rate;

solvent A: 18.2 MΩ Nanopure water + 0.05% trifluoroacetic acid (TFA), solvent B: acetonitrile + 0.05% TFA; starting condition: 90% A + 10% B, 1% per min gradient B) (Supplementary Fig. 2). cRGD-N_3 was ligated to the tension probe ligand strand via 1,3-dipolar cycloaddition reaction. Briefly, 5 nmol of alkyne ligand strand was reacted overnight with ~75 nmol of cRGD-N_3 in the presence of 0.1 M sodium ascorbate and 0.1 mM Cu-THPTA. The product was purified with a P2 size exclusion column, and then using reverse-phase HPLC with an Agilent Advanced oligo column (0.5 ml min^{-1} flow rate; solvent A: 0.1 M triethylammonium acetate (TEAA), solvent B: acetonitrile; starting condition: 90% A + 10% B, 0.5% per min gradient B) (Supplementary Fig. 2). Using this synthetic procedure (NHS-azide addition to ligand followed by 1,3-dipolar cycloaddition to alkyne DNA), any alkyne DNA could be conjugated to the cRGDfK peptide in a highly efficient manner.

Imager strands were dried and reacted overnight with a 15× excess of Cy3B-NHS dissolved in 1 µl of dimethylsulfoxide. The total reaction volume was 10 µl, composed of 1× PBS supplemented with 0.1 M $NaHCO_3$. The reaction pot was purified by a P2 size exclusion gel to remove unreacted dye followed by HPLC purification (0.5 ml min^{-1} flow rate; solvent A: 0.1 M TEAA, solvent B: acetonitrile; starting condition: 90% A + 10% B, 1% per min gradient B) to purify products (Supplementary Fig. 2).

The retention times of all products and starting reagents are shown in the HPLC spectra in Supplementary Fig. 2, and in Supplementary Table 2.

To synthesize DNA docking site-tagged phalloidin, excess TCO NHS ester was added to 20 nmol of phalloidin-amine in 20 µl of dimethylsulfoxide containing 10% 10× PBS. The solution was vortexed briefly, then reacted at 50 °C for 1 h. The product was purified by HPLC and identity was confirmed by electrospray ionization mass spectrometry. Methyltetrazine-PEG4-azide was then functionalized to alkyne-functionalized DNA using copper(I)-catalyzed azide–alkyne cycloaddition. Briefly, 1 mg of methyltetrazine-PEG4-azide was dissolved in 20 µl of 1:4 dimethylsulfoxide/H_2O and warmed to 50 °C. The copper reaction mixture was prepared in a separate tube by combining, in the following order, 1 equiv. of 20 mM $CuSO_4$, 2 equiv. of 50 mM THPTA and 5 equiv. of 50 mM ascorbic acid. The reaction mixture was then added to 15 nmol of DNA in water and warmed to 50 °C. Once warmed, the solution was added to the methyltetrazine-PEG4-azide with dropwise addition of dimethylsulfoxide to maintain solubility. The reaction proceeded at 50 °C for 2 h and the resulting product was purified using P2 gel filtration. Finally, TCO phalloidin and methyltetrazine-functionalized DNA were each dissolved in 10 µl of 10× PBS and combined to make the final DNA docking site-conjugated phalloidin. The reaction proceeded at room temperature overnight and the resulting product was purified by HPLC.

Origami design and synthesis. Single-stranded scaffold p7560 was prepared from M13 phage using a previously reported method[50,51]. A 16HB rod was designed in caDNAno, based on a 4×4-square lattice cross-section. To synthesize 16HB, a tenfold excess of staple strands was mixed with p7560 scaffold strand (10 nM) in folding buffer (5 mM Tris, 1 mM EDTA, 10 mM $MgCl_2$) with a total volume of 50 µl. The mixture was denatured at 85 °C for 10 min, followed by a slow anneal from 60 °C to 25 °C over 18 h (−1 °C per 30 min). 16HB was purified from excess staples using agarose gel electrophoresis (0.67%) in 0.5× TBE + Mg buffer (45 mM Tris, 45 mM boric acid, 1 mM EDTA, 10 mM $MgCl_2$). 16HB structures were characterized by agarose gel electrophoresis (1.5%) and negative-stain transmission electron microscopy imaging (1% uranyl formate).

Determination of DNA surface density. We adapted a surface density quantification assay that was previously published[52]. This protocol requires the preparation of a supported lipid membrane, because the bilayer structures provide a known molecular density on a glass slide surface that can be used to quantify DNA surface density. The protocol requires three main steps outlined here:

1. **Small unilamellar vesicle (SUV) preparation to determine DNA surface density.** SUVs were prepared by extrusion. 1,2-dioleoyl-*sn*-glycero-3-phosphocholine (DOPC) (850375C, Avanti Polar Lipids) and Texas Red (TR) 1,2-dihexadecanoyl-*sn*-glycero-3-phosphoethanolamine, triethylammonium salt (TR-DHPE) were mixed in ~100 µl of chloroform at 100 mol% DOPC or 99.5 mol% DOPC and 0.5 mol% TR-DHPE. Chloroform was evaporated by rotary evaporation, and lipid cakes were dried under vacuum and under ultra-high-purity nitrogen. Lipids were resuspended in water at 2 mg ml^{-1} and sonicated for 30 s before three freeze–thaw cycles. SUVs were extruded 10× in a 10-ml LIPEX Extruder (Transferra Nanosciences) fit with a 0.08-µm polycarbonate filter (WHA110604, Whatman) and a drain disc (WHA230600, Whatman). The final concentration of TR in liposomes was measured on a Thermo Scientific Nanodrop 2000c spectrophotometer.
2. **Supported lipid bilayer (SLB) preparation.** SLBs were formed in untreated glass-bottom 96-well plates (265300, Nunc). Glass was etched for 1 h in 2.6 M sodium hydroxide and washed with 5 ml of nanopure water and 5 ml of 1× PBS. TR-labeled and unlabeled SUVs were added in known ratios for ~10 min to form SLBs containing 0.01–0.06 mol% TR-DHPE. SLBs were washed with 5 ml of nanopure water and 2.5 ml of 1× PBS. SLBs were imaged in nanopure water. When used for passivation, SLBs were prepared with 100 mol% DOPC.
3. **Bulk probe density calculation.** The bulk probe density was determined by measuring the fluorescence intensity of single-stranded tension gauge tethers tagged with Cy3B and comparing this value with a fluorescence calibration curve generated by measuring the intensity of SLB standards containing TR-labeled phospholipids. The TR-DHPE number per micrometer was estimated using the DOPC footprint in a membrane[53]. The Cy3B-DNA and TR fluorescence were equated by the F-factor, $F_{Cy3B\text{-}TR}$, which is defined by:

$$F_{Cy3B\text{-}TR} = \frac{I_{Cy3B\text{-}DNA}}{I_{TR\text{-}DHPE}}$$

$F_{Cy3B\text{-}TR}$ was determined by measuring the intensity of free dye-labeled DNA ($I_{Cy3B\text{-}DNA}$) and TR-labeled SUVs ($I_{TR\text{-}DHPE}$) in nanopure water at 50–500 nM fluorophore. To avoid surface adsorption, glass was passivated with a DOPC SLB before buffer exchanging with the sample. In-solution images were collected 5 µm above the surface.

Statistics. Two-tailed, two-sample *t*-tests were used to compare: (1) the means of the localization density on sf-tPAINT surface versus the strained surface (Extended Data Fig. 1); and (2) the means of the localization density on the accumulated-tPAINT surface versus sf-tPAINT surface (Extended Data Fig. 3). Two-way analysis of variance was used to compare: (1) the mean of the ratios of cell/background density (Extended Data Fig. 5); and (2) the means of background localization produced by scrambled imager versus tPAINT imager (Extended Data Fig. 6).

Human subjects statement. All procedures using donor-derived human platelets were approved by the Institutional Review Board of Children's Healthcare of Atlanta/Emory University. Written, informed consent was received from participants before their inclusion in studies.

Reporting Summary. Further information on research design is available in the Nature Research Reporting Summary linked to this article.

Data availability

Data supporting the main figures in this work are available at https://doi.org/10.15139/S3/WB168Q. Other data that support the findings of this study are available from the corresponding authors upon reasonable request. Further information regarding the experimental design may be found in the Nature Research Reporting Summary.

Code availability

Filtering algorithms are derived from published methods[31]. The code is available from the corresponding author upon reasonable request.

References

48. Pan, H., Xia, Y., Qin, M., Cao, Y. & Wang, W. A simple procedure to improve the surface passivation for single molecule fluorescence studies. *Phys. Biol.* **12**, 045006 (2015).
49. Hua, B. et al. An improved surface passivation method for single-molecule studies. *Nat. Methods* **11**, 1233–1236 (2014).
50. Bazrafshan, A. et al. Tunable DNA origami motors translocate ballistically over µm distances at nm/s speeds. *Angew. Chemie Int. Ed. Engl.* **59**, 9514–9521 (2020).
51. Douglas, S. M., Chou, J. J. & Shih, W. M. DNA-nanotube-induced alignment of membrane proteins for NMR structure determination. *Proc. Natl Acad. Sci. USA* **104**, 6644–6648 (2007).
52. Galush, W. J., Nye, J. A. & Groves, J. T. Quantitative fluorescence microscopy using supported lipid bilayer standards. *Biophys. J.* **95**, 2512–2519 (2008).
53. Vacklin, H. P., Tiberg, F. & Thomas, R. K. Formation of supported phospholipid bilayers via co-adsorption with β-D-dodecyl maltoside. *Biochim. Biophys. Acta* **1668**, 17–24 (2005).

Acknowledgements

J.M.B., A.T.B. and R.G. acknowledge NSF GRFP grant no. 1444932. J.M.B. acknowledges NCI fellowship grant no. F99CA234959. A.T.B. acknowledges NCI fellowship grant no. F99CA245789. A.V.K. acknowledges NIH grant no. F31 F31CA243502. M.E.Q. acknowledges NIH grant no. F31 F31HL134241. H.O. acknowledges a grant from The Naito Foundation and a postdoctoral fellowship from The Uehara Memorial Foundation. B.G.P. acknowledges NIH grant no. HL117061. R.L. acknowledges NIH grant no. HL082808. Y.K. acknowledges NIH grant no. 1R21AI135753–01. A.L.M. acknowledges NSF CAREER grant no. 1832100. A.L.M. and K.S. acknowledge NIH grant no. R01GM131099. K.S. acknowledges NIH grant no. R01GM124472. We thank V.P.-Y. Ma for helpful discussions.

Author contributions

J.M.B., H.S., Y.K. and K.S. designed the study. J.M.B., H.S., A.B., A.V.K., R.L.B., H.O. and R.G. performed experiments. J.M.B. and H.S. analyzed data. Y.D. and T.M. designed and synthesized DNA origami. E.M.Q., B.G.P. and R.L. assisted with platelet experiments. A.T.B. performed computational modeling. R.M. assisted with probe design. F.S. and R.J. assisted with design and optimization of speed-optimized tPAINT probes. A.L.M., Y.K. and K.S. supervised the study. J.M.B., H.S. and K.S. wrote the manuscript.

Competing interests

The authors declare no competing interests.

Additional information

Extended data is available for this paper at https://doi.org/10.1038/s41592-020-0929-2.

Supplementary information is available for this paper at https://doi.org/10.1038/s41592-020-0929-2.

Correspondence and requests for materials should be addressed to K.S.

Reprints and permissions information is available at www.nature.com/reprints.

Peer review information Rita Strack was the primary editor on this article and managed its editorial process and peer review in collaboration with the rest of the editorial team.

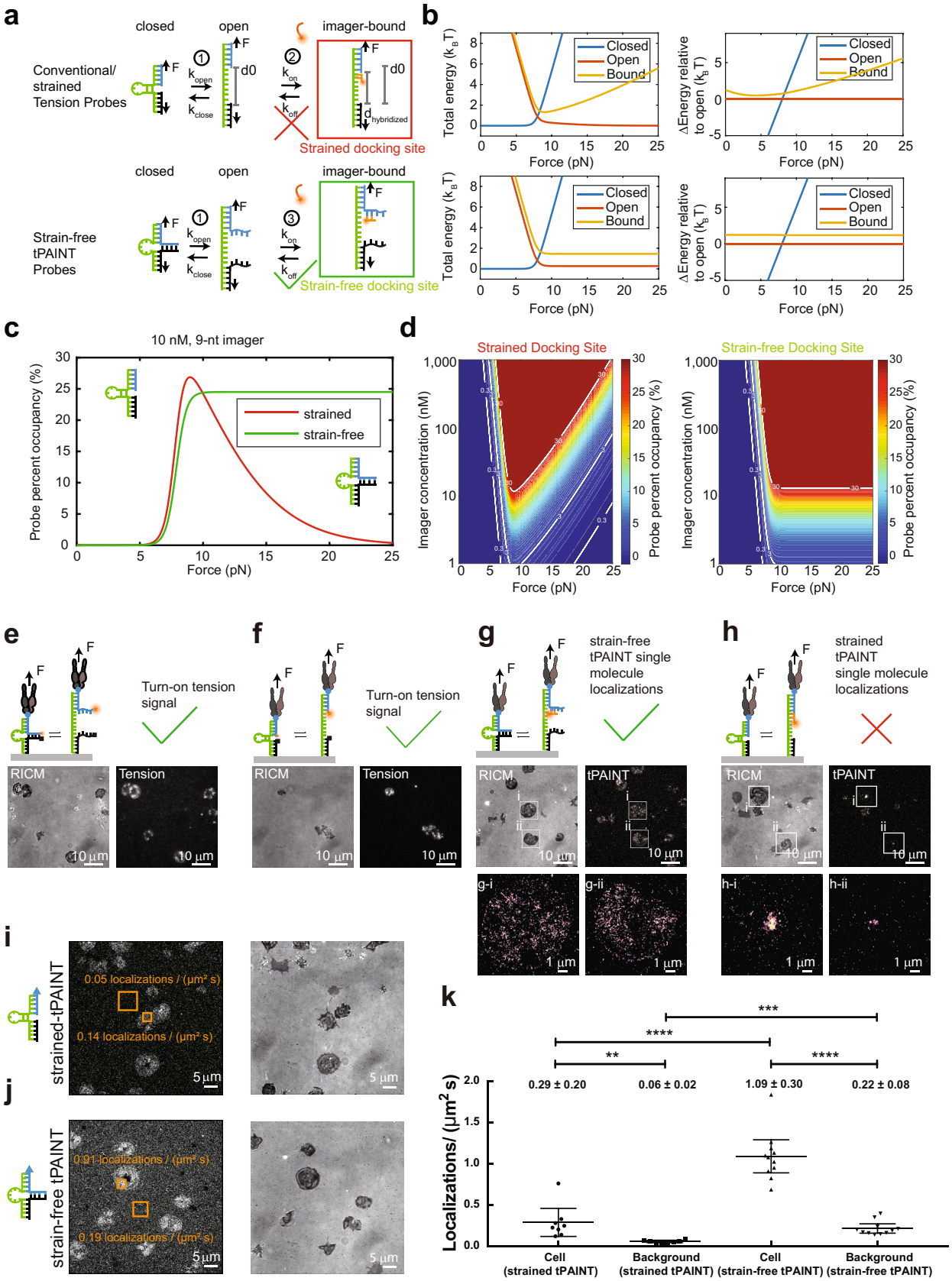

Extended Data Fig. 1 | See next page for caption.

Extended Data Fig. 1 | Strain-free (sf)-tPAINT probe modeling and testing shows significant advantages over conventional hairpin probes (strained-tPAINT probes). a, Schematic of binding of imagers to strain-free (sf-tPAINT) and conventional/strained probes. **b**, Total energy and change in energy as a function of applied force as predicted by the kinetic model described in Supplementary Note 2. **c**, Docking site occupancy as a function of applied *F* for strained (red), and sf-tPAINT probes (green) at 10 nM imager and (**d**) for varying imager concentration. Force impedes imager binding to strained but not sf-tPAINT probes. **e–h**, Experimental validation that sf-tPAINT probes outperform strained probes. **e**, Strain-free and **f**, conventional (strained) probes tagged with Cy3B-BHQ2 report pN tension as fluorescence. Images representative of $n=6$ (**e**) and $n=3$ experiments (**f**). **g**, Strain-free and **h**, conventional/strained probes were incubated with 10 nM Cy3B-imager and imaged in TIRF excitation. These images were reconstructed from 5000 frames of single molecule localizations. Data shown in **g**, **h** are from paired experiments using different fluidic channels on the same glass coverslip and using the same platelet donor. The results shown are representative of $n=3$ experiments. **i–k,** Quantification of single molecule localizations ($\mu m^{-2}\ s^{-1}$) for strained and sf-tPAINT probes. Results are representative of $n=4$ (11 images) independent experiments for strained tPAINT surfaces and $n=6$ independent sf-tPAINT surfaces (8 images). Data in **k** is displayed as mean with 95% CI. Cell (strained tPAINT): Mean= 0.29, 95% CI 0.12–0.46; Background (strained tPAINT): Mean= 0.06, 95% CI 0.04–0.07; Cell (sf-tPAINT): Mean= 1.09, 95% CI 0.89–1.29; Background (sf-tPAINT): Mean= 0.22, 95% CI 0.16–0.27. To determine the statistical significance, student t-test was applied to the data and the exact *p*-values are calculated (2 tailed, 2 sample). Cell (strained tPAINT) vs Background (strained tPAINT): 1.5×10^{-2}, Cell (sf-tPAINT) vs Background (sf-tPAINT): 7.2×10^{-7}, Cell (strained tPAINT) vs Cell (sf-tPAINT): 2.3×10^{-6}, Background (strained tPAINT) vs Background (sf-tPAINT): 8.4×10^{-5}.

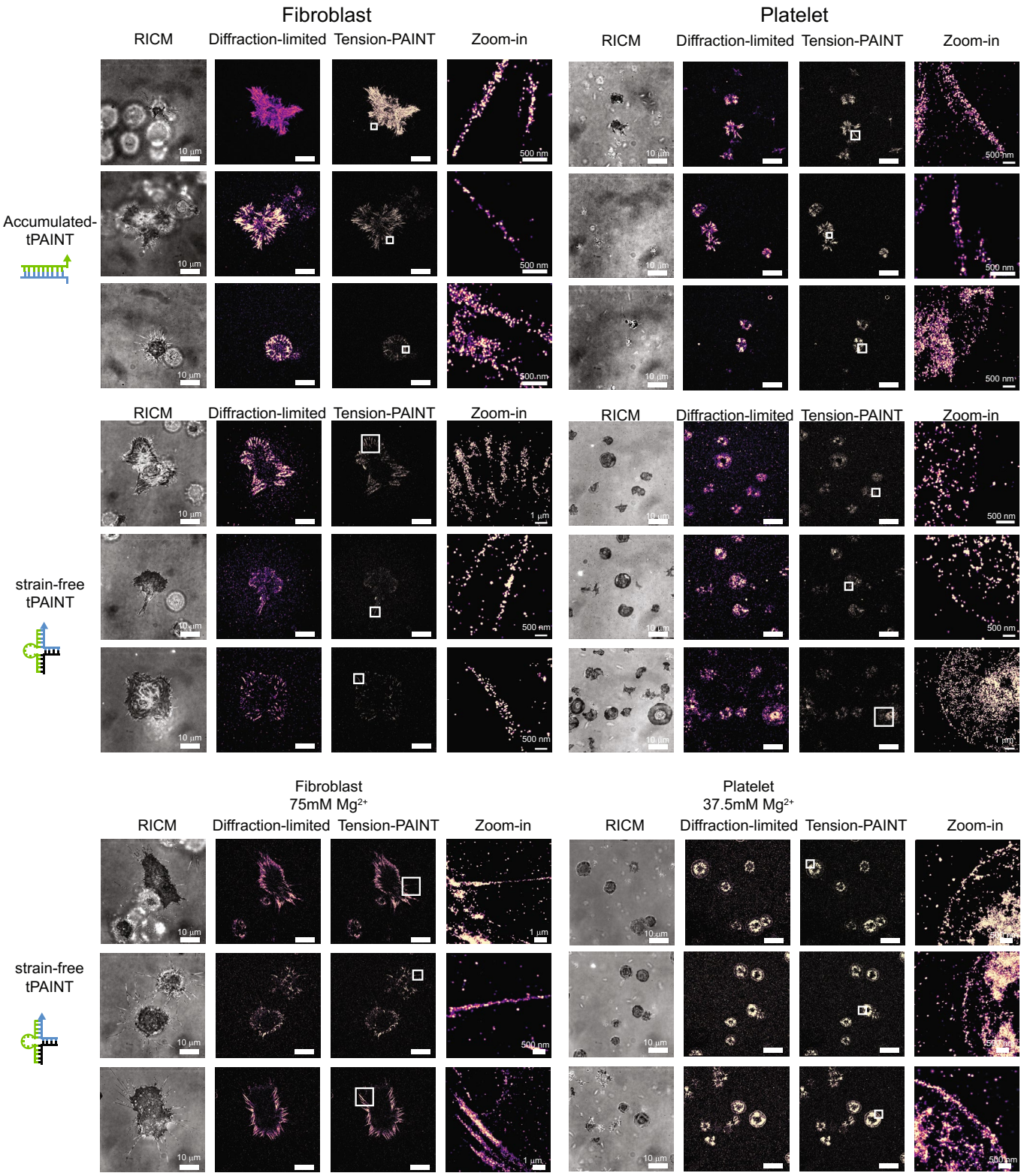

Extended Data Fig. 2 | Collage of examples showing accumulated-tPAINT and ~8.5 pN sf-tPAINT integrin tension maps for MEFs and human platelets. Representative examples of images for MEF GFP-vinculin cells and human platelets displayed with a 5x density filter and kinetic filter. Images are representative of: 12pN T_{tol} accumulated-tPAINT maps, platelets, $n = 8$ replicates (22 images), and fibroblasts, $n = 9$ replicates (24 images); 7.3pN sf-tPAINT maps, fibroblasts, $n = 3$ experiments (cell culture media, 0.8 mM Mg^{2+}), 8.5pN sf-tPAINT platelet maps, $n = 4$ experiments (Tyrode's buffer + 2 mM Mg^{2+}); sf-tPAINT maps in media supplemented with Mg^{2+}, $n = 3$ independent platelet experiments (37.5 mM Mg^{2+}) from 3 different donors (8 images) and $n = 4$ fibroblast experiments (75 mM Mg^{2+} 10 images).

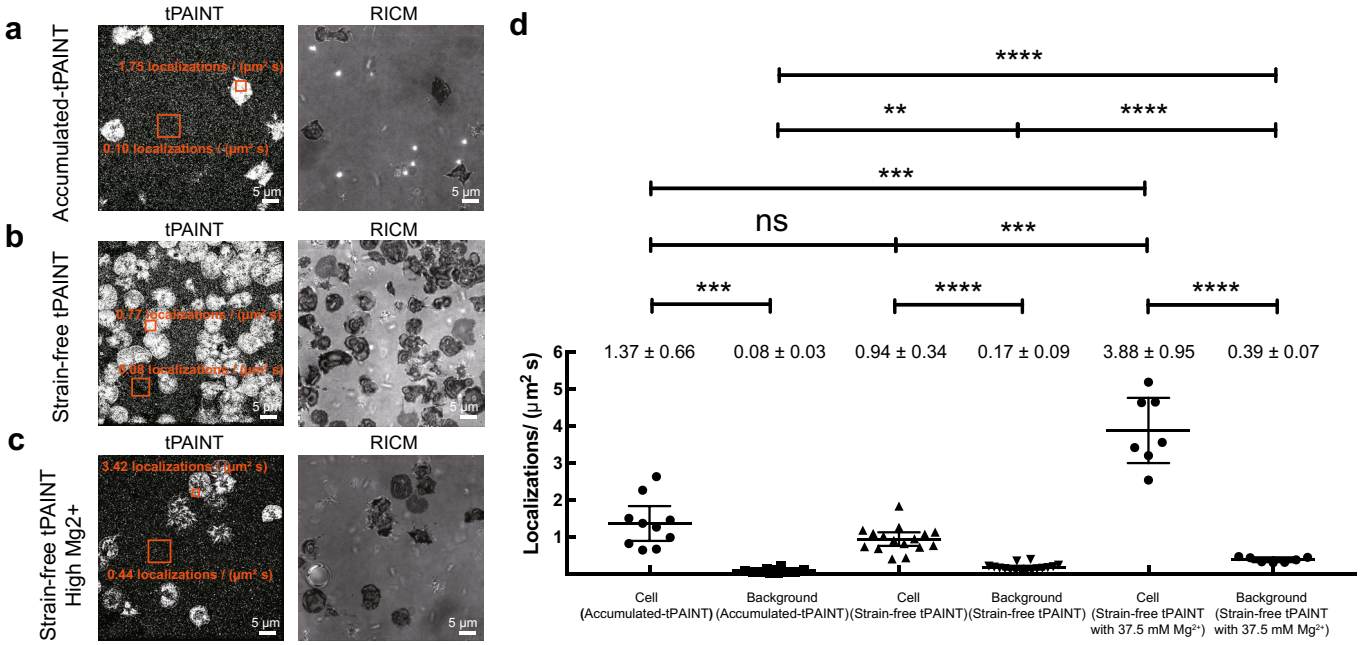

Extended Data Fig. 3 | Mechanoselection produces a signal-to-background ratio of up to 10 for sf-tPAINT probes and 17 for accumulated-tPAINT probes. Human platelets were seeded on surfaces presenting cRGD-modified (**a**) 12pN T_{tol} accumulated-tPAINT probes at low [Mg^{2+}], (**b**) sf-tPAINT probes at low [Mg^{2+}], and (**c**) sf-tPAINT probes with 37.5 mM Mg^{2+}. Note that the images displayed are raw-unfiltered single molecule localizations of tPAINT images with the contrast adjusted to emphasize the background localizations. **d**, The average per image localizations ($\mu m^{-2}s^{-1}$) for both the background and for the mechanical "footprint" of platelets (3 ROIs per image) is plotted. Results were obtained from $n=4$ independent accumulated-tPAINT surfaces, $n=8$ sf-tPAINT surfaces and $n=3$ high [Mg^{2+}] sf-tPAINT surfaces (10 images for accumulated-tPAINT, 16 images for strain-free, 7 images for high [Mg^{2+}] strain-free). Mean ± standard deviation is noted above each category, error bar is mean with 95% CI. Cell (accumulated-tPAINT): Mean= 1.37, 95% CI 0.89–1.84; Background (accumulated-tPAINT): Mean= 0.08, 95% CI 0.02–0.04; Cell (strain-free tPAINT): Mean= 0.94, 95% CI 0.76–1.13; Background (sf-tPAINT): Mean= 0.17, 95% CI 0.12–0.22. Cell (high [Mg^{2+}] sf-tPAINT): Mean= 3.88, 95% CI 3.00–4.76; Background (high [Mg^{2+}] sf-tPAINT): Mean= 0.39, 95% CI 0.32–0.45. Student's *t*-test was (2-tailed, 2 sample) was applied to determine significance. Cell (accumulated-tPAINT) vs Background (accumulated-tPAINT): $p=1.6\times10^{-4}$, Cell (strain-free) vs Background (strain-free): $p=1.3\times10^{-7}$, Cell (High [Mg^{2+}] strain-free) vs Background (High [Mg^{2+}] strain-free): $p=6.5\times10^{-5}$, Cell (accumulated-tPAINT) vs Cell (strain-free): $p=8.5\times10^{-2}$, Cell (accumulated-tPAINT) vs Cell (High [Mg^{2+}] strain-free): $p=1.3\times10^{-4}$, Cell (strain-free) vs Cell (High [Mg^{2+}] strain-free): $p=1.2\times10^{-4}$, Background (accumulated-tPAINT) vs Background (strain-free): $p=8.4\times10^{-5}$. Background (accumulated-tPAINT) vs Background (strain-free): $p=5.2\times10^{-3}$, Background (accumulated-tPAINT) vs Background (High [Mg^{2+}] strain-free): $p=1.1\times10^{-6}$, Background (strain-free) vs Background (High [Mg^{2+}] strain-free): $p=1.7\times10^{-5}$.

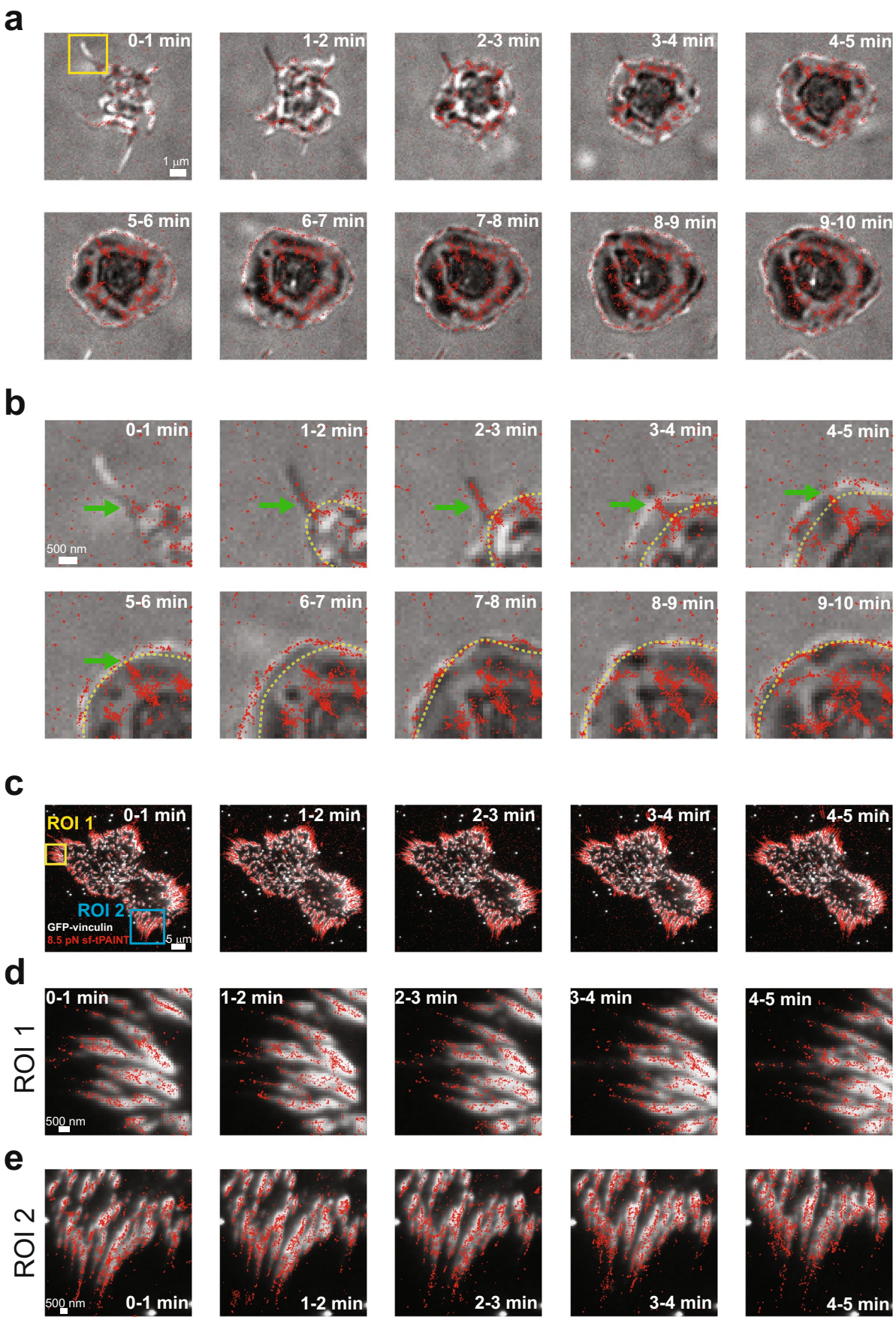

Extended Data Fig. 4 | See next page for caption.

Extended Data Fig. 4 | Analysis of lamellipodial and focal adhesion dynamics using time resolved 8.5pN sf-tPAINT. a, 8.5 pN tPAINT integrin forces (red points) and RICM (grey scale image) were simultaneously imaged in a spreading human platelet. Each RICM image was collected at the beginning of the time window, while the 8.5pN sf-tPAINT data represents the accumulated signal in a 60 sec interval. **b**, Zoom-in images of the region highlighted with yellow box in (**a**). The green arrow denotes the formation of a filopodium and the force associated with extension of this structure. For frames corresponding to minutes 1–10, the cell edge in the previous frame is highlighted with a dashed yellow line. Note that the filopodial forces are still resolved even after lamellipodial spreading. **c**, Full cell view of a mouse embryonic fibroblast (MEF); **d**, **e**, show zoom-ins of the regions highlighted with yellow and blue boxes, respectively. Note that the focal adhesion (as indicated by the vinculin-GFP data) is offset from the mechanical localizations. The tension signal extends beyond the tip of the focal adhesions away from the cell body, and this is clear both in the full view of the cell (**c**), as well as the zoom in panels (**d**) and (**e**). This could be consistent with previous reports by Waterman and colleagues which found that the centroid of focal adhesion traction stresses is consistently ~1μm distal to the focal adhesion centroid[29]. This finding is also consistent with previous publications from our lab[28], and the diffraction limited tension reported in Supplementary Fig. 3 of this work. Data shown is representative of: platelets, $n = 3$ independent experiments (5 images); fibroblasts, $n = 3$ independent experiments (5 images).

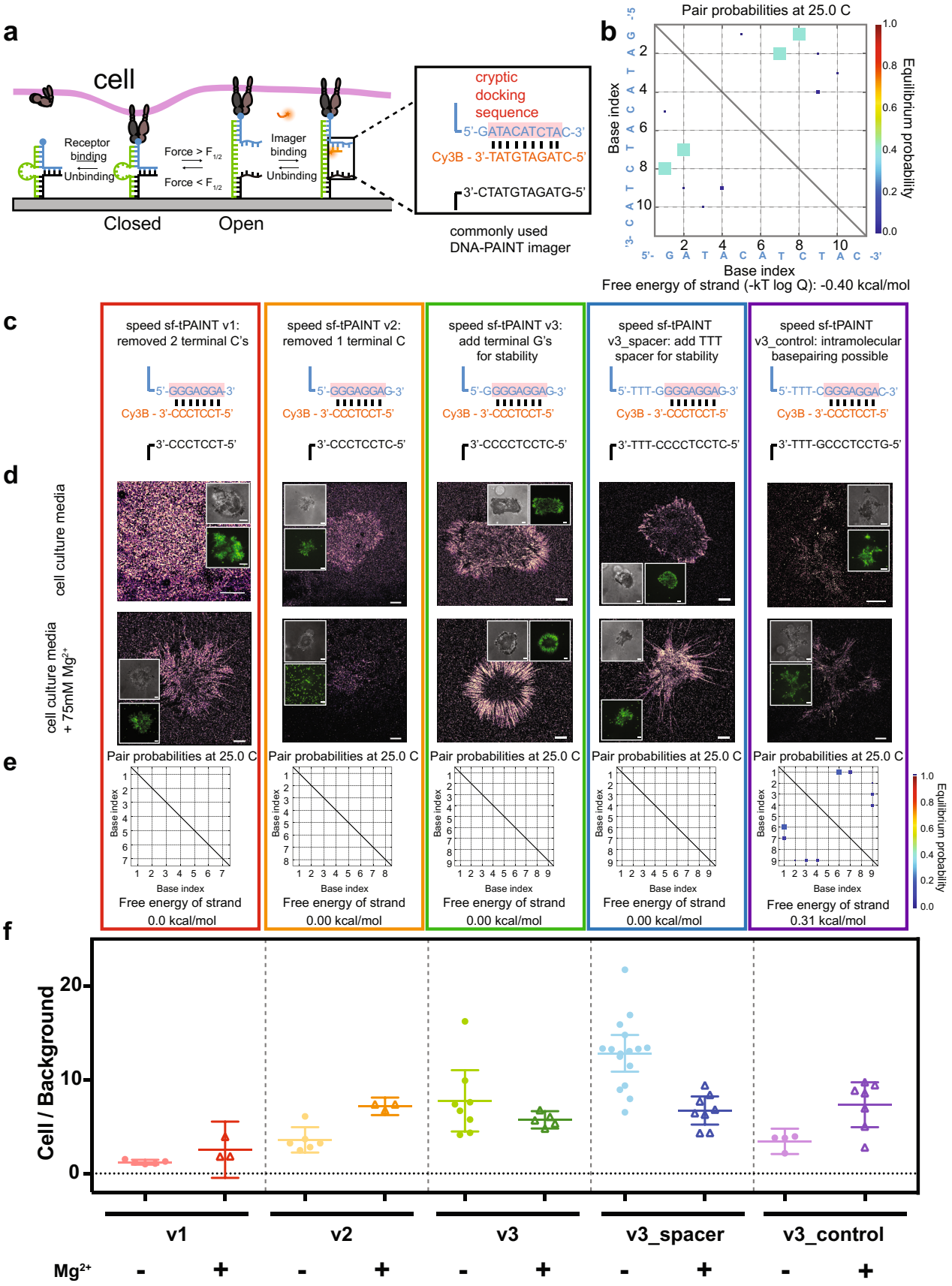

Extended Data Fig. 5 | See next page for caption.

Extended Data Fig. 5 | Design of speed-optimized strain-free tPAINT probes. a, Schematic of sf-tPAINT probes. **b**, NUPACK modeling of self-base-pairing propensity of the imager. **c**, Sequences/designs of speed-optimized sf-tPAINT docking sites (blue strand) that avoid self-interaction. Imager docking site highlighted in pink. **d**, Representative speed sf-tPAINT images of MEF GFP-vinculin cells imaged in cell culture media (~0.8 mM Mg^{2+}) and in 75 mM Mg^{2+} supplemented media. **e**, NUPACK modeling of speed sf-tPAINT probes. **f**, Ratio of tPAINT localizations versus background localizations. Each point in (**f**) is a single cell. Number of replicates: v1_no Mg^{2+} (5 cells, $n=3$ experiments), v1_ Mg^{2+} (3 cells, $n=3$ experiments), v2_no Mg^{2+}(6 cells, $n=3$ experiments), v2_Mg^{2+} (3 cells, $n=3$ experiments), v3_no Mg^{2+} (8 cells, $n=3$ experiments), v3_Mg^{2+}(5 cells, $n=3$ experiments), and v3_spacer_no Mg^{2+}(16 cells, $n=4$ experiments), v3_spacer_Mg^{2+} (8 cells, $n=4$ experiments), v3_control_no Mg^{2+} (4 cells, $n=4$ experiments), v3_control_Mg^{2+} (7 cells, $n=3$ experiments). All scale bars are 5 μm. Data were compared via a 2-way ANOVA. v3_spacer (in the no added Mg^{2+} case) is statistically different from v1 ($p=5.3\times10^{-10}$), v2 ($p=6.4\times10^{-8}$), v3 ($p=0.0022$), and v3_control ($p=2.2\times10^{-6}$). The v3_spacer exhibits the greatest signal-to-noise ratio. Data in **f** is displayed as mean with 95% CI. v1 (no Mg^{2+}) Mean= 1.21, CI 0.96–1.46, sd 0.20; v1 (Mg^{2+}) Mean= 2.54, CI 0.47–5.55, sd 1.21; v2 (no Mg^{2+}) Mean= 3.60, CI 2.24–4.95, sd 1.29; v2 (Mg^{2+}) Mean= 7.17, CI 6.23–8.11, sd 0.38; v3 (no Mg^{2+}) Mean= 7.76, CI 4.49–11.02, sd 3.90; v3 (Mg^{2+}) Mean= 5.73, CI 4.81–6.66, sd 0.74; v3_spacer (no Mg^{2+}) Mean= 12.82, CI 10.86–14.78, sd 3.67; v3_spacer (Mg^{2+}) Mean= 6.72, CI 5.22–8.22, sd 1.80; v3_control (no Mg^{2+}) Mean= 3.43, CI 2.09–4.78, sd 0.84; v3_control (Mg^{2+}) Mean= 7.34, CI 4.95–9.74, sd 2.59.

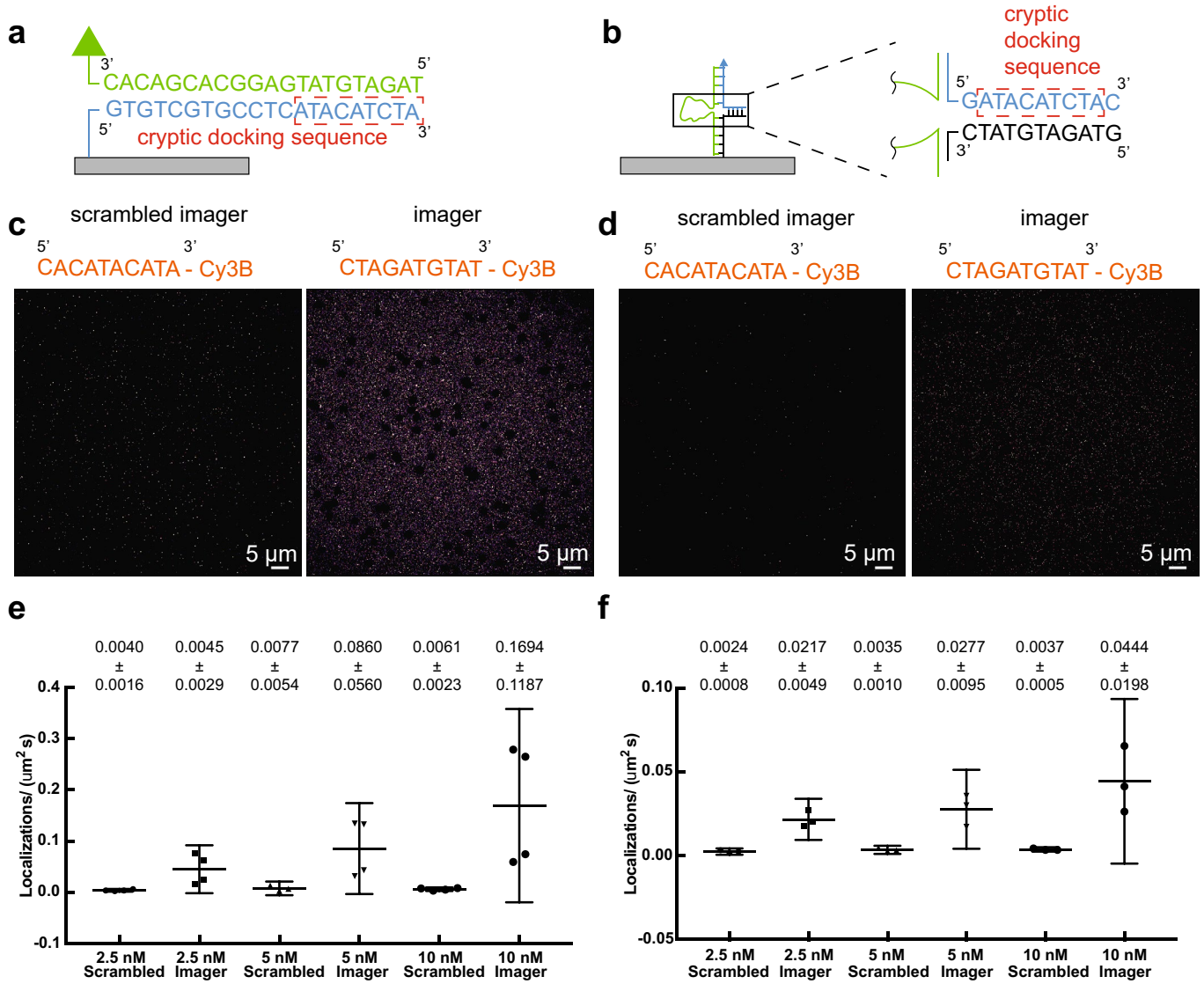

Extended Data Fig. 6 | Background localizations are imager-sequence specific. a, Accumulated-tPAINT or (**b**) sf-tPAINT surfaces were incubated with scrambled-imager and specific imager. **c**, Representative images compiled from 2000 frames of single molecule localization for accumulated-tPAINT surfaces and (**d**) sf-tPAINT probes incubated with 5 nM scrambled and specific imagers. The average localizations ($\mu m^{-2}s^{-1}$) were quantified at 2.5, 5, and 10 nM scrambled and specific imagers for (**e**) accumulated-tPAINT ($n = 4$ independent experiments) and (**f**) sf-tPAINT surfaces (n = 3 independent experiments). Localization density was computed for 5 regions per image to compute an average (black points). Mean ± standard deviation is noted above each category. Error bars are 95% CI. 2.5 nM (accumulated-tPAINT, Scrambled): Mean= 0.0040, 95% CI 0.0015–0.0066; 2.5 nM (accumulated-tPAINT, Specific): Mean= 0.045, 95% CI −0.0017–0.092; 5 nM (accumulated-tPAINT, Scrambled): Mean= 0.0077, 95% CI −0.0057–0.02101; 5 nM (accumulated-tPAINT, Specific): Mean= 0.086, 95% CI −0.0032–0.17; 10 nM (accumulated-tPAINT, Scrambled): Mean= 0.0061, 95% CI 0.0025–0.0097; 10 nM (accumulated-tPAINT, Specific): Mean= 0.17, 95% CI −0.020–0.36; 2.5 nM (sf-tPAINT, Scrambled): Mean= 0.0024, 95% CI 0.00057–0.0043; 2.5 nM (sf-tPAINT, Specific): Mean= 0.022, 95% CI 0.0094–0.034; 5 nM (sf-tPAINT, Scrambled): Mean= 0.0035, 95% CI 0.0011–0.0059; 5 nM (sf-tPAINT, Specific): Mean= 0.028, 95% CI 0.0041–0.051; 10 nM (sf-tPAINT, Scrambled): Mean= 0.0037, 95% CI 0.0024–0.0050; 10 nM (sf-tPAINT, Specific): Mean= 0.044, 95% confidence interval −0.0048–0.094. Data were compared via a 2-way ANOVA. For localization on accumulated-tPAINT probe surface: 2.5 nM scramble versus 2.5 specific ($p = 0.9968$); 5 nM scramble versus 5 nM specific ($p = 0.7527$); 10 nM scramble is statistically different than 10 nM specific ($p = 0.0115$). For localization on sf-tPAINT probe surface: 2.5 nM scramble versus 2.5 specific ($p = 0.3153$); 5 nM scramble versus 5 nM specific ($p = 0.1051$); 10 nM scramble is statistically different than 10 nM specific ($p = 0.0023$).

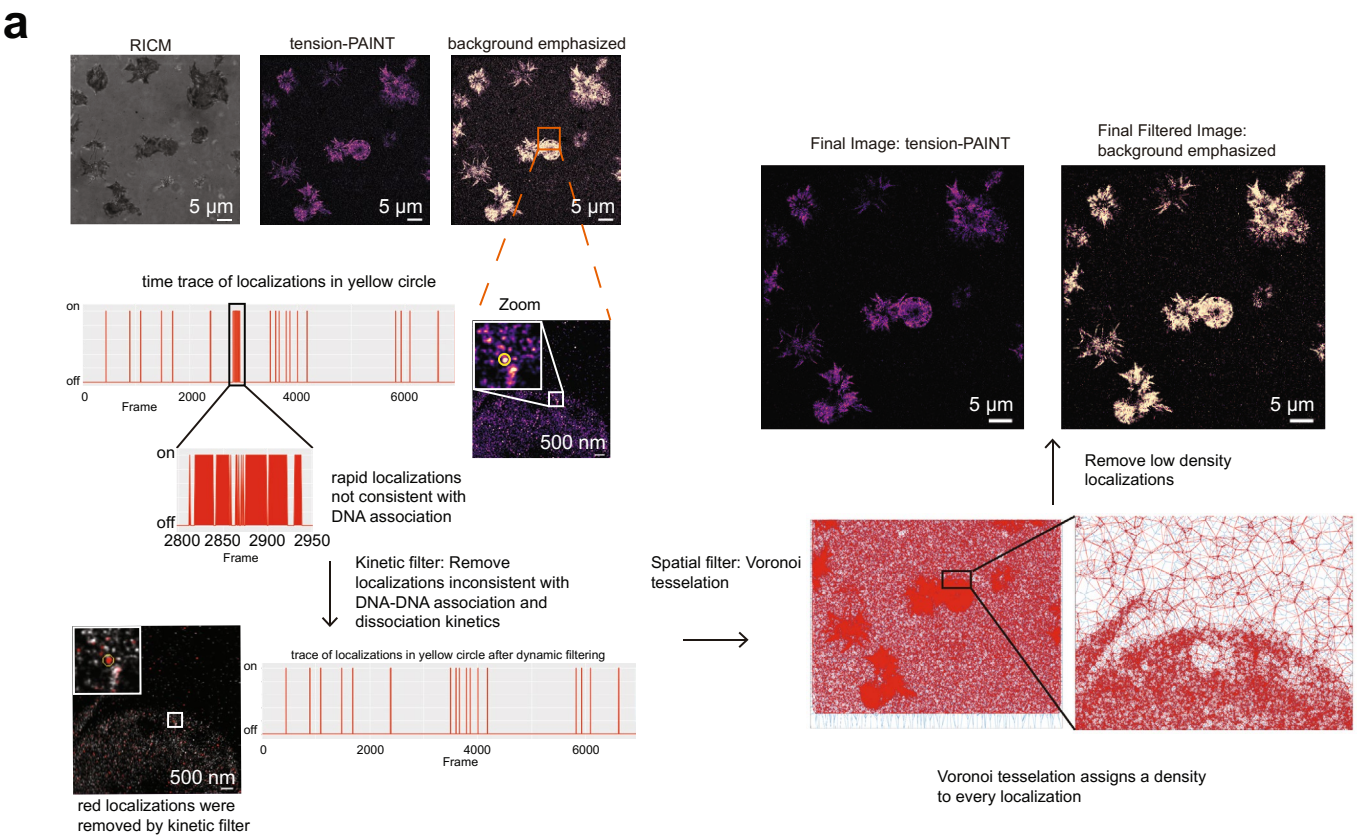

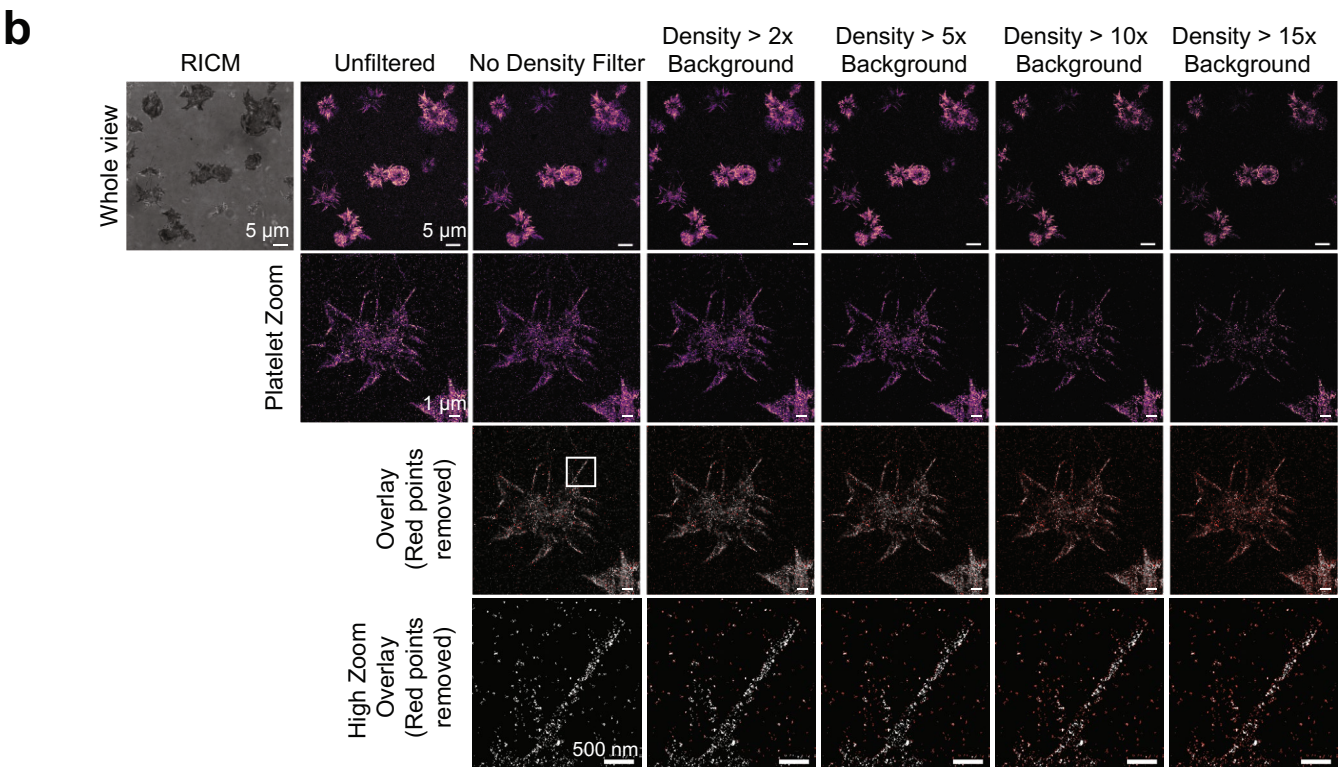

Extended Data Fig. 7 | See next page for caption.

Extended Data Fig. 7 | Schematic showing the filtering algorithm and effect of filtering on representative data. a, First, tPAINT data was subjected to kinetic and density-based filtering prior to analysis. Kinetic filtering was accomplished via a 25-frame moving window of time traces of localizations within 35 nm oversampled pixels. If 14 events occurred within the 25-frame window (corresponding to 2.8 s of accumulated single molecule bond lifetime), all the component events were removed. Second, a Voronoi-tessellation assigned a polygon, comprised of all points closer to that localization than to any other localization, to each tPAINT localization. A local "density" was computed for each localization. Localizations with density lower than 2x, 5x, or 10x the background density were removed to produce the final tPAINT image. **b**, Demonstration of how increasingly stringent density filters (2x, 5x, 10x, and 15x the background localization density) affects the tPAINT signal. In the overlay, red points indicate localization density that has been removed by the density filter while white regions indicate localizations that passed the density threshold. The high zoom overlay displays the raw localizations as points, not gaussians. At the highest density-based filter settings, localizations on the edge of the filopodial extension are removed (high zoom overlay, 10x and 15x density filter). Scale bars: whole image view, 5 μm; platelet zoom view, 1 μm; high zoom view; 500 nm. The processing described in (**a**, **b**) above were applied to all tPAINT data reported in this manuscript: platelets sf-tPAINT $n = 3$ independent experiments, 3 donors, 8 images; fibroblasts $n = 4$ experiments, 10 images; accumulated-tPAINT platelets, $n = 8$ replicates, 3 donors, 22 images; $n = 9$ replicates, 24 images.

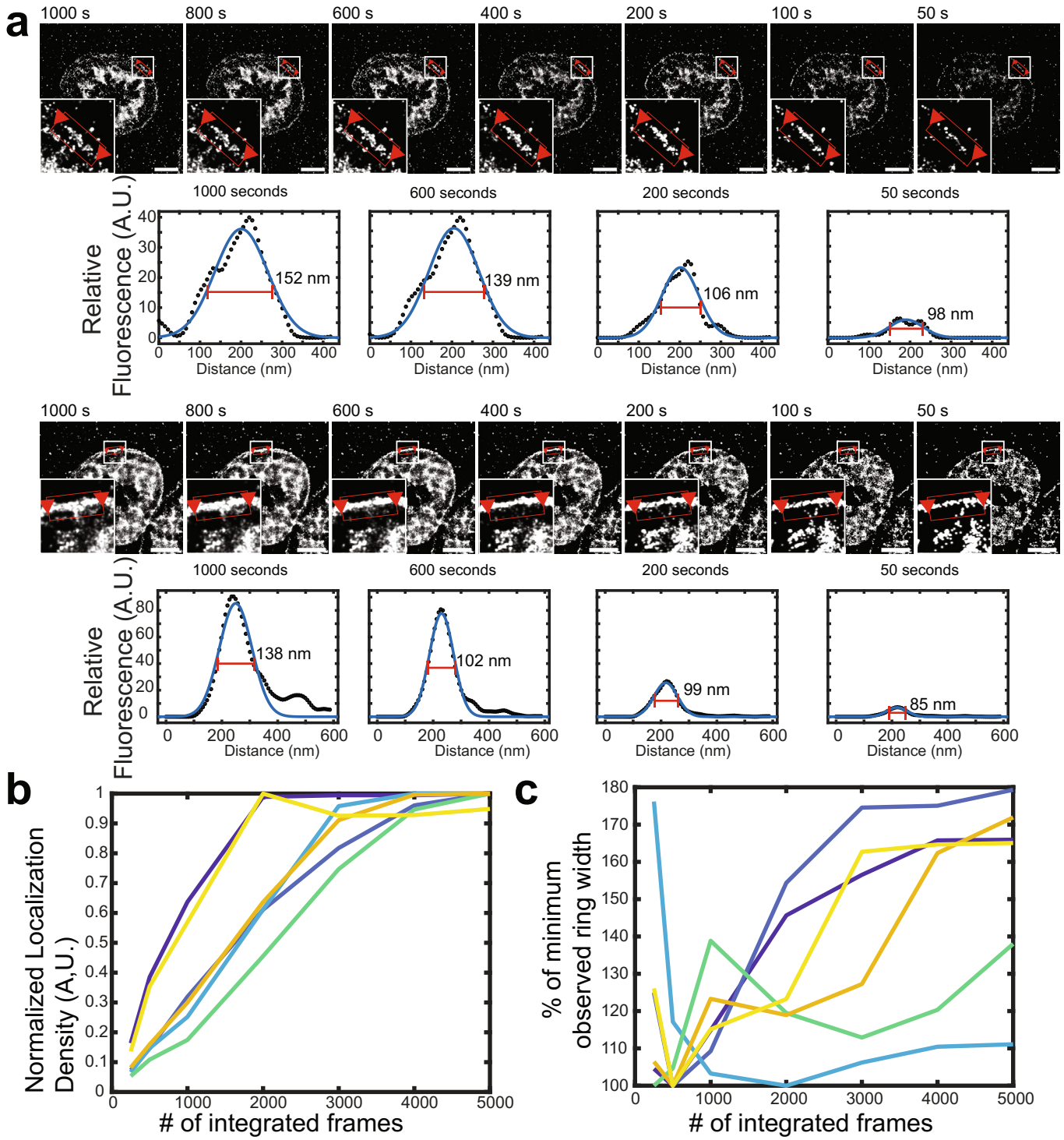

Extended Data Fig. 8 | Cellular tension feature dimensions depend on the imaging window in sf-tPAINT. a, Live-cell sf-tPAINT imaging of platelet tension displayed using different time windows (ranging from 50 sec to 1000 sec). The apparent length or width of cellular tension features depends on the number of frames that are integrated to produce a super-resolved image. To demonstrate this point, we rendered the lamellipodial edge of 3 human platelets (from $n = 3$ independent experiments, 2 platelets shown) and measured the apparent width of the lamellipodial edge tension ring as tPAINT data is integrated over various time windows. Super-resolved tPAINT images were rendered as greyscale images, and ring width was measured via linescan analysis (black dots). The data were fit to a gaussian via Matlab's curvefitting tool (blue line). The measured FWHM of the fitted gaussians depends on the number of frames integrated to produce the super-resolved tPAINT image. **b**, Plot showing that the localization density generally increased with increasing number of integrated frames. Each colored line shows a unique ROI. **c**, Plot showing the relation between the FWHM of the tension ring and the number of integrated frames. The data shown are from 3 human platelets from $n = 3$ independent experiments (2 linescans per platelet). In principle, it is desirable to use the minimum number of frames possible to render an image in order to minimize feature blurring due to cellular dynamics during the imaging window; however, image quality decreases, with localizations becoming more punctate, when fewer frames are integrated. To produce high-quality tPAINT images, these considerations must both be balanced. All scale bars are 2 μm.

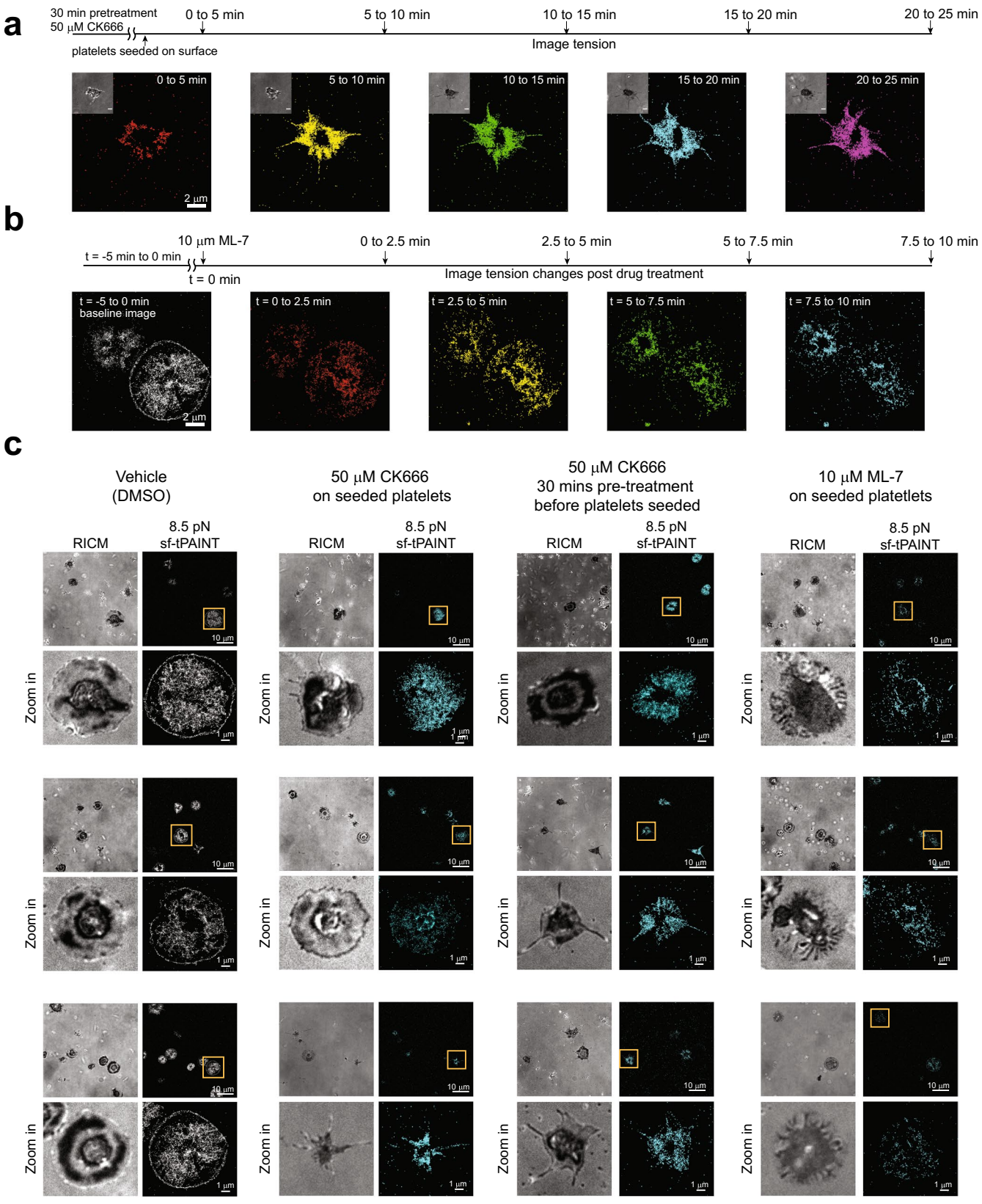

Extended Data Fig. 9 | Collage of examples showing sf-tPAINT of human platelets treated with cytoskeletal inhibitors. a, Time-resolved 8.5 pN tPAINT of platelets pre-treated with 50 μM CK666 for 30 min before being seeded on sf-tPAINT probes. **b**, Time-resolved 8.5 pN tPAINT image of platelet before and after treatment with 10μM ML-7 (MLCK inhibitor). **c**, Representative examples of images for cells treated with inhibitors displayed with a 5x density filter and kinetic filter. Human platelets treated with vehicle (DMSO) as control (n = 3 independent experiments), human platelets treated with CK666 (50 μM) after being seeded on the surface (n = 2 independent experiments), human platelets pretreated with CK666 (50 μM) for 30 min before being seeded on the surface (n = 3 independent experiments), human platelets treated with ML-7 (MLCK inhibitor, 10 μM) after being seeded on the surface (n = 3 independent experiments). Three examples are shown for each condition.

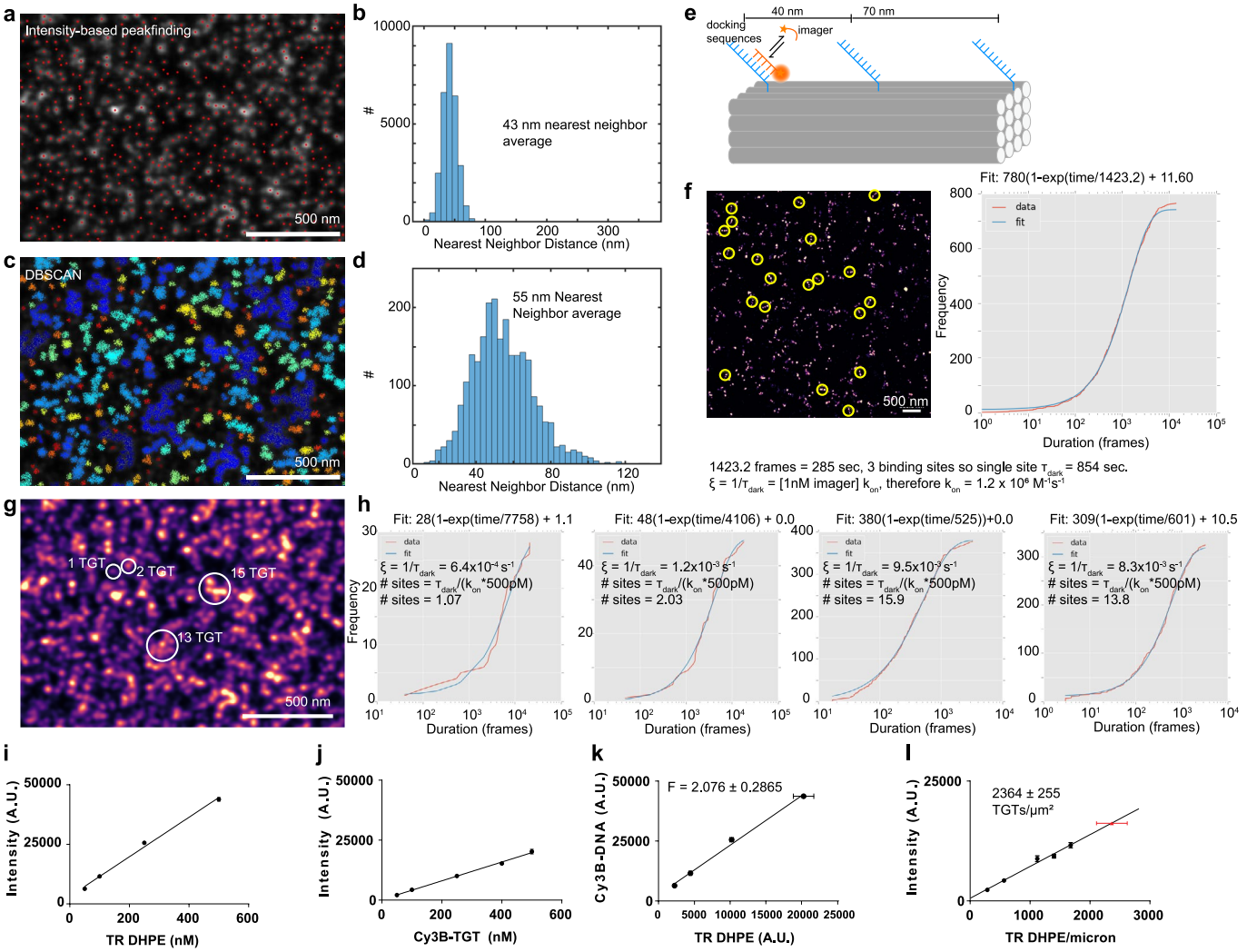

Extended Data Fig. 10 | Surface density of tPAINT probes on the coverslip. a, DNA-PAINT imaging of docking site coated surfaces (500 pM Cy3B-imager, 150,000–200,000 frames). Intensity-based peakfinding identified localization clusters (red dots). **b**, Histogram of nearest-neighbor distances reveals average cluster-cluster distance of 43 nm. **c**, Alternate DBSCAN clustering algorithm (20 localization minimum, 0.05 pixel search radius) identified clusters (displayed as colored dots). **d**, Nearest-neighbor histogram of the centroids of the clusters identified in **c** reports 55 nm average nearest-neighbor distance. Images in **a** and **c** are representative of $n = 3$ independent experiments. **e-h**, Variations in cluster localization density suggested peakfinding/DBSCAN did not identify individual docking sites. To count individual docking sites, we performed quantitative-PAINT (qPAINT). **e**, Calibration DNA origami used for calculating imager influx rate and (**f**) DNA-PAINT image of origami. Images were acquired at 1, 2.5, and 5 nM Cy3B imager ($n = 3$ independent experiments). Plot depicts cumulative distribution function of dark times between imager binding (red) and exponential fit (blue) for selected origamis (yellow circles). This analysis calculated k_{on} as 1.2×10^6 $M^{-1}s^{-1}$. **g**, **h**, qPAINT of tPAINT surface reveal dense, heterogeneous clusters of docking sites on the surface (**i–l**). Quantitative measurements of the surface density of probes were performed to supplement qPAINT and clustering measurements. **i**, **j**, Fluorescence intensity versus concentration for Texas-red (TR) tagged phospholipid vesicles (5 measurements per concentration per experiment, $n = 3$ independent experiments), and soluble Cy3B-DNA (5 measurements per concentration per experiment, $n = 2$ independent experiments). Error bars are standard deviation. **k**, F factor calibration (ratio of TR:Cy3B fluorescence). Error bars calculated from the propagated standard deviation of Cy3B-DNA/TR-DHPE measurements. **l**, To calculate tPAINT probe density, fluorescence measurements of Cy3B-DNA tPAINT surfaces (5 measurements from each of $n = 3$ independent experiments) were converted into density via the F factor. tPAINT probe density is 2364 +/−255 probes per square micron (mean +/-propagated SEM from Cy3B and TR measurements).

nature research

Corresponding author(s): Khalid Salaita

☐ Initial submission ☐ Revised version ☒ Final submission

Life Sciences Reporting Summary

Nature Research wishes to improve the reproducibility of the work that we publish. This form is intended for publication with all accepted life science papers and provides structure for consistency and transparency in reporting. Every life science submission will use this form; some list items might not apply to an individual manuscript, but all fields must be completed for clarity.

For further information on the points included in this form, see Reporting Life Sciences Research. For further information on Nature Research policies, including our data availability policy, see Authors & Referees and the Editorial Policy Checklist.

Experimental design

1. Sample size

Describe how sample size was determined.

Platelet data:
Platelet data from 3 experiments (6 donors) is reported for the 37.5mM Mg2+ speed PAINT experiments, and from 3 experiments (6 donors) for low Mg2+ data. An experiment is defined as an individually prepared tPAINT DNA-probe functionalized surface with a separate biological replicate (separate donor). Platelet images were acquired for ~30-90 min per surface, allowing time for approximately 1-3 tPAINT image acquisitions. The sample size was defined by the number of images that could be acquired during that time. This sample size is sufficient to demonstrate the robustness and reproducibility of the tPAINT method. The use of 6 human donors ensures the results obtained from our imaging method are robust and biologically general.

Fibroblast data:
75mM Mg2+ speed PAINT fibroblast data originates from 4 experiments, while low Mg2+ data originates from 3 experiments, where an experiment is defined as an individually prepared, tPAINT DNA-probe functionalized surface with data being collected on different days utilizing different passages of the MEF GFP vinculin cell line. Images were acquired for ~45 min per surface, allowing approximately 1-4 tPAINT image acquisitions during that time. The number of fibroblasts that were imaged during that window defined the sample size. This sample size is sufficient to demonstrate the reproducibility and robustness of the technique.

2. Data exclusions

Describe any data exclusions.

Images where cells failed to adhere to the substrate, or where cells failed to produce increased localizations over the background were excluded from analysis. These exclusions only occurred for tPAINT experiments conducted in cell culture media/tyrode's buffer unsupplemented with Mg2+. All data collected with the speed-optimized tPAINT probes, and with Mg2+ supplemented buffer are reported. See "Replication" section for further details.

3. Replication

Describe whether the experimental findings were reliably reproduced.

37.5/75 mM Mg2+ speed PAINT experiments were extremely reproducible (100% success rate). Low Mg2+ experiments with fibroblasts were poorly reproducible (~30% success rate, success being defined as images in which the cell produced increased localizations over the background) with the real time tPAINT probe. ~90% of low Mg2+ platelet experiments succeeded. TGT experiments were extremely reproducible, (100% success rate). Successful experiments are defined as experiments where cells produced increased localization density over the background. Each figure caption describes the exact number of independent replicates that were performed.

4. Randomization

Describe how samples/organisms/participants were allocated into experimental groups.

We did not randomize samples because randomization is not necessary to demonstrate the capability of tPAINT to measure pN receptor forces with

nanoscale resolution. The results were not used to distinguish between samples. Individual experiments were grouped for statistical analysis.

5. Blinding

Describe whether the investigators were blinded to group allocation during data collection and/or analysis.

No group allocation was performed, therefore no blinding to group assignments was required.

Note: all studies involving animals and/or human research participants must disclose whether blinding and randomization were used.

6. Statistical parameters

For all figures and tables that use statistical methods, confirm that the following items are present in relevant figure legends (or in the Methods section if additional space is needed).

n/a	Confirmed
☐	☒ The exact sample size (*n*) for each experimental group/condition, given as a discrete number and unit of measurement (animals, litters, cultures, etc.)
☐	☒ A description of how samples were collected, noting whether measurements were taken from distinct samples or whether the same sample was measured repeatedly
☐	☒ A statement indicating how many times each experiment was replicated
☐	☒ The statistical test(s) used and whether they are one- or two-sided (note: only common tests should be described solely by name; more complex techniques should be described in the Methods section)
☐	☒ A description of any assumptions or corrections, such as an adjustment for multiple comparisons
☐	☒ The test results (e.g. *P* values) given as exact values whenever possible and with confidence intervals noted
☐	☒ A clear description of statistics including central tendency (e.g. median, mean) and variation (e.g. standard deviation, interquartile range)
☐	☒ Clearly defined error bars

See the web collection on statistics for biologists for further resources and guidance.

Software

Policy information about availability of computer code

7. Software

Describe the software used to analyze the data in this study.

Programs written in MATLAB 2019a were used for the analysis of all data. The algorithms for processing the data are not novel, and are derived from published procedures. The code used is available upon reasonable request.

Nikon Elements (64 bit) v. 4.40.00 (build 1084)

Picasso version 2.8

Statistical analyses were performed in Graphpad v. 8.4.2.679

For manuscripts utilizing custom algorithms or software that are central to the paper but not yet described in the published literature, software must be made available to editors and reviewers upon request. We strongly encourage code deposition in a community repository (e.g. GitHub). *Nature Methods* guidance for providing algorithms and software for publication provides further information on this topic.

Materials and reagents

Policy information about availability of materials

8. Materials availability

Indicate whether there are restrictions on availability of unique materials or if these materials are only available for distribution by a for-profit company.

The DNA tension probes that enable tPAINT require custom synthesis, but are assembled from materials that are commercially available.

9. Antibodies

Describe the antibodies used and how they were validated for use in the system under study (i.e. assay and species).

N/A

10. Eukaryotic cell lines

a. State the source of each eukaryotic cell line used.

Mouse embryonic fibroblast cells stably expressing GFP-vinculin were a gift from the lab of Prof. Andres Garcia (originally generated in the lab of Andres Garcia).

b. Describe the method of cell line authentication used.

The cell lines have not been authenticated.

c. Report whether the cell lines were tested for mycoplasma contamination.

The cell lines were not tested for mycoplasma contamination.

d. If any of the cell lines used are listed in the database of commonly misidentified cell lines maintained by ICLAC, provide a scientific rationale for their use.

No commonly misidentified cell lines were used.

Animals and human research participants

Policy information about studies involving animals; when reporting animal research, follow the ARRIVE guidelines

11. Description of research animals

Provide details on animals and/or animal-derived materials used in the study.

N/A

Policy information about studies involving human research participants

12. Description of human research participants

Describe the covariate-relevant population characteristics of the human research participants.

All procedures using donor-derived human platelets were approved by the Institutional Review Board of Children's Healthcare of Atlanta/Emory University (IRB # IRB00006228). Written, informed consent was received from participants prior to their inclusion in studies. 5 males (age 25-40) and one female (age 25-40) were used in this study.